Title:

The pigtail macaque (*Macaca nemestrina*) model of COVID-19 reproduces diverse clinical outcomes and reveals new and complex signatures of disease

Alexandra Melton[1,2], Lara A Doyle-Meyers[1,9], Robert V Blair[1], Cecily Midkiff[1], Hunter J Melton[3], Kasi Russell-Lodrigue[1], Pyone P Aye[1,9], Faith Schiro[1], Marissa Fahlberg[1], Dawn Szeltner[1], Skye Spencer[1], Brandon J Beddingfield[1], Kelly Goff[1], Nadia Golden[1], Toni Penney[1], Breanna Picou[1], Krystle Hensley[1], Kristin E Chandler[1], Jessica A Plante[4], Kenneth S Plante[4], Scott C Weaver[4], Chad J Roy[1,8], James A Hoxie[5], Hongmei Gao[6], David C Montefiori[6], Joseph L Mankowski[7], Rudolf P Bohm[1,9], Jay Rappaport[1,8], Nicholas J Maness[1,8,*]

[1]Tulane National Primate Research Center, Covington, Louisiana

[2]Biomedical Science Training Program, Tulane University School of Medicine, New Orleans, Louisiana

[3]Florida State University, Department of Statistics, Tallahassee, Florida

[4]World Reference Center for Emerging Viruses and Arboviruses, Institute for Human Infections and Immunity, University of Texas Medical Branch, Galveston, Texas

[5]Perelman School of Medicine, University of Pennsylvania, Philadelphia, Pennsylvania

[6]Duke University Medical Center, Duke Human Vaccine Institute, Durham, North Carolina

[7]Department of Molecular and Comparative Pathobiology, Johns Hopkins School of Medicine, Baltimore, Maryland

[8]Department of Microbiology and Immunology, Tulane University School of Medicine, New Orleans, Louisiana

[9]Department of Medicine, Tulane University School of Medicine, New Orleans, Louisiana

*To whom correspondences should be addressed

Abstract

The novel coronavirus SARS-CoV-2, the causative agent of COVID-19 disease, has killed over four million people worldwide as of July 2021 with infections rising again due to the emergence of highly transmissible variants. Animal models that faithfully recapitulate human disease are critical for assessing SARS-CoV-2 viral and immune dynamics, for understanding mechanisms of disease, and for testing vaccines and therapeutics. Pigtail macaques (PTM, *Macaca nemestrina*) demonstrate a rapid and severe disease course when infected with simian immunodeficiency virus (SIV), including the development of severe cardiovascular symptoms that are pertinent to COVID-19 manifestations in humans. We thus proposed this species may likewise exhibit severe COVID-19 disease upon infection with SARS-CoV-2. Here, we extensively studied a cohort of SARS-CoV-2-infected PTM euthanized either 6- or 21-days after respiratory viral challenge. We show that PTM demonstrate largely mild-to-moderate COVID-19 disease. Pulmonary infiltrates were dominated by T cells, including CD4+ T cells that upregulate CD8 and express cytotoxic molecules, as well as virus-targeting T cells that were predominantly CD4+. We also noted increases in inflammatory and coagulation markers in blood, pulmonary pathologic lesions, and the development of neutralizing antibodies. Together, our data demonstrate that SARS-CoV-2 infection of PTM recapitulates important features of COVID-19 and reveals new immune and viral dynamics and thus may serve as a useful animal model for studying pathogenesis and testing vaccines and therapeutics.

Introduction

In late 2019, a novel coronavirus was found circulating in humans in China. This virus showed substantial genomic similarities with the severe acute respiratory syndrome coronavirus (SARS-CoV) that caused an outbreak and panic in 2003[1] in addition to a number of bat sarbecoviruses[2]; hence, it was named SARS-CoV-2[3]. SARS-CoV-2 is the causative agent of COVID-19 disease and a worldwide pandemic that has killed more than four million persons to date including over 600,000 deaths in the United States. Though most infected individuals exhibit no or mild symptoms, a subset experience severe complications, including highly elevated pro-inflammatory cytokines and coagulation biomarkers, acute respiratory distress syndrome (ARDS), and death[4–9]. Most available data suggest that the intensity of the immune response plays a role in determining COVID-19 severity and progression, with severe disease occurring approximately 3-to-4-weeks after initial symptoms.[10,11]. Thus, a deep understanding of the immunopathologic mechanisms of disease in those with advanced disease and of viral clearance in asymptomatic infection and those with mild disease is critical for the development of next generation therapies and vaccines.

Animal models that faithfully recapitulate human disease are needed to assess the roles of particular cell subsets in disease etiology. Various species of nonhuman primates can be infected by SARS-CoV-2 and exhibit disease ranging from mild to severe[12–16]. The use of timed infections with well characterized viral stocks in animals with relatively high genetic similarity with humans allows the dissection of immune responses with nuance and detail not possible in humans. The most widely used species of NHP for COVID-19 research has been the rhesus macaque (*Macaca mulatta*). This model has proved valuable for testing vaccines as viral infection dynamics in this species are robust and well-studied and therefore can be compared between treatment groups. However,

SARS-CoV-2-induced disease in this species is generally mild and does not recapitulate the more severe disease seen in a subset of humans. Thus, multiple NHP models are needed to capture the spectrum of disease seen in humans. In this study, we infected pigtail macaques (PTM, *Macaca nemestrina*) with SARS-CoV-2 (WA1/2020 isolate) to assess this novel animal model of COVID-19 disease.

PTM are a unique and valuable animal model for other viral diseases. Simian immunodeficiency virus (SIV) infection of rhesus macaques (RhM) is the most widely used nonhuman primate model of HIV/AIDS and is used widely for testing vaccines and cure strategies. However, SIV-associated disease in RhM can take up to several years to develop, somewhat limiting their use for studying disease mechanisms. In contrast, infection of PTM with the same viral isolates leads to rapid disease development with enhanced cardiovascular manifestations relative to RhM, which is of particular relevance to COVID-19 disease[17–20]. Thus, we proposed that SARS-CoV-2 infection of PTM may likewise lead to accelerated COVID-19 disease or demonstrate immune features of disease not detected in other animal models. If so, this species will be valuable for assessing COVID-19 disease mechanisms and for testing novel vaccines and therapeutics. We tracked viral and immune dynamics through the course of infection in a cohort of PTM. We found that disease in this model largely mirrored that observed in RhM but with unique immune features, such as pulmonary infiltration of CD4+ T cells that exhibit antiviral and cytotoxic functions, as is seen in COVID-19 patients[21]. Together, our data characterize, in depth, a novel animal model that may prove useful for assessing moderate COVID-19 disease mechanisms and testing new therapeutics.

Materials and Methods

Animal cohort, viral inoculations, and procedures

Four male pigtail macaques (PTM), between the ages of 5 and 6 years old (Table S1), were exposed to $1x10^6$ $TCID_{50}$ of SARS-CoV-2 USA WA1/2020 (World Reference Center for Emerging Viruses and Arboviruses, Galveston, TX) through both intranasal and intratracheal inoculation. The viral stock was sequenced and determined to have no mutations at greater than 5% of reads that differed from the original patient isolate. Pre- and post-exposure samples included blood, bronchoalveolar lavage (BAL), and mucosal swabs (nasal, pharyngeal, rectal, and bronchial brush). Physical examination and imaging (radiography Figure S1) were conducted before viral exposure and weekly after exposure. Animals were monitored for 6 (n=2) or 21 (n=2) days before euthanasia and tissue harvest. At necropsy, samples from each of the major lung lobes (left and right, cranial, middle, and caudal lobes) were collected in TRIzol (Invitrogen, Lithuania) and fresh frozen at -80°C. The remainder of the lung lobes were infused and then immersed in formalin fixative. The rest of the necropsy was performed routinely with collection of tissues from all major organs in DMEM media, fresh frozen, or in formalin fixative.

Animal ID	Sex	Age (y)	Weight (kg)
MA27	Male	6.07	7.55
MA30	Male	5.61	5.80
MA24	Male	5.64	8.40
MA28	Male	5.81	8.60

Ethics Statement

Pigtail macaques used in this study were purpose bred at the University of Washington National Primate Research Center for experiments. Macaques were housed in compliance with the NRC Guide for the Care and Use of Laboratory Animals and the Animal Welfare Act. Animal experiments were approved by the Institutional Animal Care and Use Committee of Tulane University (protocol P0451). The Tulane National Primate Research Center (TNPRC) is fully accredited by AAALAC International, Animal Welfare

Assurance No. A3180-01. During the study, animals were singly housed indoors in climate-controlled conditions with a 12/12-light/dark cycle. All the animals on this study were monitored twice daily to ensure their welfare. Any abnormalities, including those of appetite, stool, and behavior, were recorded and reported to a veterinarian. The animals were fed commercially prepared nonhuman primate diet twice daily. Supplemental foods were provided in the form of fruit, vegetables, and foraging items as part of the TNPRC environmental enrichment program. Water was available ad libitum through an automatic watering system. The TNPRC environmental enrichment program is reviewed and approved by the IACUC semi-annually. Veterinarians in the TNPRC Division of Veterinary Medicine have established procedures to minimize pain and distress using several approaches. Animals were anesthetized with ketamine-HCl (10 mg/kg) or tiletamine/zolazepam (3-8 mg/kg) prior to all procedures. Preemptive and post procedural analgesia (buprenorphine 0.01 mg/kg or buprenorphine sustained-release 0.2 mg/kg SQ) was used for procedures that would likely cause more than momentary pain or distress in humans undergoing the same procedures. The above listed anesthetics and analgesics were used to minimize pain and distress in accordance with the recommendations of the Weatherall Report. The animals were euthanized at the end of the study using methods consistent with recommendations of the American Veterinary Medical Association (AVMA) Panel on euthanasia and per the recommendations of the IACUC. Specifically, the animals were anesthetized with tiletamine/zolazepam (8 mg/kg IM) and given buprenorphine (0.01 mg/kg IM) followed by an overdose of pentobarbital sodium. Death was confirmed using auscultation to confirm the cessation of respiratory and circulatory functions and by the lack of corneal reflexes.

Isolation of Viral RNA

The *Quick*-RNA Viral Kit (Zymo Research, Irvine, CA) was used to isolate viral RNA (vRNA) from mucosal swab and bronchial brush samples collected in 200 µL DNA/RNA Shield 1X (Zymo Research, Irvine, CA) following the manufacturer's protocol. Briefly, 400 µL DNA/RNA viral buffer was added to the swab samples. In a modification to the manufacturer's protocol, swabs were transferred directly to the Zymo spin column for centrifugation. The vRNA was eluted in 50 µL elution buffer.

Viral RNA Quantification by Quantitative Real-Time PCR

Quantification of viral RNA was performed as described[22] using the CDC N1 primers/probe for quantification of total viral RNA and with primers/probe specific for the nucleocapsid subgenomic RNA to provide an estimate of replicating virus. Specifically, vRNA was quantified using the QuantStudio 6 Real-Time PCR System (Applied Biosystems, Waltham, MA). Five microliters vRNA was added in duplicate to a 0.1 mL 96-well MicroAmp fast optical reaction plate (Applied Biosystems, REF# 4346906). For genomic vRNA quantification, the 2019-nCoV RUO Kit (Integrated DNA Technologies, Coralville, IA) was used, according to the manufacturer's protocol, to target the N1 amplicon of the N gene along with TaqPath 1-Step RT-qPCR Master Mix (Applied Biosystems Waltham, MA). For the subgenomic assay, a forward primer targeting the subgenomic leader sequence and a reverse primer/probe (Integrated DNA Technologies, Waltham, MA) designed to target the N gene, was used along with the TaqPath Master Mix mentioned above. Fifteen microliters of the respective master mix was added to each well and run using the following conditions: 25°C for 2 minutes, 50°C for 15 minutes, 95°C for 2 minutes followed by 40 cycles of 95°C for 3 seconds and 60°C for 30 seconds. In vitro transcribed RNA was quantified and diluted to known copy numbers and used to generate the genomic and subgenomic standard curves. Both

genomic and subgenomic viral copy numbers were calculated by plotting Cq values from unknown samples against the respective standard curve. Positive, negative, and non-template controls were analyzed along with each set of samples.

Isolation of PBMCs

Peripheral blood mononuclear cells (PBMCs) were isolated from whole blood using SepMate-50 Isolation tubes (Stem Cell Technologies, Vancouver, Canada) per the manufacturer's protocol. Cells were counted using a Cellometer Auto 2000 (Nexcelom, Lawrence, MA), resuspended in Bambanker cell freezing medium (GC Lymphotec, Tokyo, Japan) at approximately $1x10^7$ cells/mL and cryopreserved at -80°C.

ELISA assays

D-dimer levels in sodium citrate plasma samples were measured via an enzyme-linked immunosorbent assay (ELISA) (Ray Biotech, Peachtree Corners, GA) per the manufacturer's protocol. Samples were diluted 600,000-fold and plated in duplicate. Plates were analyzed using the GloMax Explorer plate reader (Promega, Madison, WI) and GraphPad Prism (GraphPad Software version 9, LaJolla, California). Heatmap was generated using Microsoft Excel. Data was normalized by dividing raw data values from Day 6, 14 and 21 by the baseline value for each animal.

Kynurenine and tryptophan levels in plasma were measured using commercially available enzyme-linked immunosorbent assays (Rocky Mountain Diagnostics, Colorado Springs, CO) per the manufacturer's protocol. The GloMax Explorer plate reader (Promega, Madison, WI) along with GraphPad Prism v9 were used to analyze the plates.

Quantification of Inflammatory Cytokines and Coagulation Biomarkers

BioLegend's bead-based immunosorbent assays were used to measure inflammatory cytokines in serum (LegendPlex NHP Inflammation Panel, BioLegend, San Diego, CA) and coagulation biomarkers in sodium citrate plasma (LegendPlex Human Fibrinolysis Panel). Serum and plasma samples were diluted 4-fold and 10,000-fold, respectively, and assayed in duplicate. Results were read using a MacsQuant 16 Flow Cytometer (Miltenyi Biotec) and LegendPlex's online data analysis tool (Qognit). Heatmap was generated using Microsoft Excel. Data was normalized by dividing raw data values from Day 6, 14 and 21 by the baseline value for each animal.

Flow Cytometry Analysis

Phenotypic and intracellular cytokine analysis of mononuclear cells (MNC) isolated from blood and bronchoalveolar lavage (BAL) was performed using antibodies against markers listed in Supplementary Tables 2-4. Briefly, cells were washed and counted with the Cellometer Auto 2000 (Nexcelom Bioscience, Lawrence, MA). Cells were then pelleted and resuspended in Live/Dead stain cocktail (50 µL PBS + 0 .5 µL live/dead stain per test) (Fixable Aqua Dead Cell Stain Kit, Invitrogen, Lithuania) and incubated in the dark for 20 minutes. Cells were washed in PBS supplemented with 2% FBS, pelleted, resuspended, and incubated in surface-stain cocktail consisting of 50µL BD Horizon Brilliant Violet Stain Buffer (BD Bioscience, Franklin Lakes, NJ) plus antibodies (see Supplementary Tables 2-4) for 20 minutes in the dark. Cells were washed in PBS with 2% FBS, pelleted, then resuspended in 200 µL BD Cytofix/Cytoperm solution (BD Biosciences, Franklin Lakes, NJ) and incubated in the dark for 20 minutes. Cells were washed in BD Perm/Wash Buffer (BD Biosciences, Franklin Lakes, NJ), pelleted, and resuspended in intracellular-staining cocktail consisting of 100 µL BD Perm/Wash Buffer plus antibodies according to Supplementary Tables 2-4 and incubated for 20 minutes in

the dark. Finally, cells were then washed, pelleted, and resuspended in 200 µL 1x BD Stabilizing Fixative (BD Biosciences, Franklin Lakes, NJ).

Monocyte Cytokine Expression

To measure monocyte cytokine expression, MNCs from blood and BAL were washed and counted (Cellometer Auto 2000, Nexcelom Bioscience, Lawrence, MA), pelleted, and then resuspended in DMEM (Gibco, Grand Island, NY) with 5% Anti-Anti (Gibco, Grand Island, NY) at $1x10^6$ cells/mL. Cells were stimulated with lipopolysaccharide at 10 ng/mL (Sigma, St Louis, MO) and incubated with 1 µL/mL Brefeldin-A (BioLegend, San Diego, CA) for 4-6 hours at 37°C, 5% CO_2. Cells were then stained following the procedure described above with antibodies listed in the Monocyte Panel (Table S2).

T cell Cytokine Expression

MNCs from BAL were counted, washed, pelleted, and resuspended in DMEM with 5% Anti-Anti at $1x10^6$ cells/mL. T cell cytokine expression was measured by stimulating MNCs with cell stimulation cocktail (Biolegend, San Diego, CA) for 4-6 hours at 37°C, 5% CO_2. To measure T cell responses to SARS-CoV-2 antigens, MNCs from blood and BAL were washed, pelleted and resuspended in DMEM with 5% Anti-Anti and 10% FBS at $1x10^6$ cells/mL followed by overnight stimulation at 37°C, 5% CO_2 with either cell stimulation cocktail or with one of the following viral peptide pools obtained through BEI Resources, NIAID, NIH: Peptide Array, SARS Coronavirus Nucleocapsid Protein (NR-52419), Spike Glycoprotein (NR-52402), Membrane Protein (NR-53822), or Envelope Protein (NR-53822) along with Brefeldin-A. Cells were stained as described above using the antibodies listed in the T cell panel (Table S4).

All samples were acquired on a LSRFortessa Cell Analyzer (BD Biosciences, Franklin Lakes, NJ) using BD FACSDIVA 8.0.1 software. Approximately $1x10^6$ cells were acquired from each sample. Data was analyzed using FlowJo version 10.7.1 for MAC (Becton Dickinson and Company, Ashland, OR). SARS-CoV-2 antigen specific T cell response figures (9A&B) were generated using the Matlab based tool cyt3[23]. Data was transformed using arcsin 150. Cytokine expression was measured in FlowJo and, when applicable, applied to cyt3 generated figures. t-distributed stochastic neighbor embedding (tSNE) analysis was performed in FlowJo 10.7.1, nightingale rose plots were generated in R using the ggplot2 package, radial plots were generated in Microsoft Excel.

Histopathology and Immunohistochemistry

Zinc-formalin fixed tissues were processed routinely, embedded in paraffin and cut in to 5 µm sections for hematoxylin and eosin (H&E) or immunohistochemical (IHC) staining. For H&E staining, tissue samples were collected in Zinc formalin (Anatech, Sparks, NV) and immersion fixed for a minimum of 72 hours before being washed and dehydrated using a Thermo Excelsior AS processor. Upon removal from the processor, tissues were transferred to a Thermo Shandon Histocentre 3 embedding station where they were submersed in warm paraffin and allowed to cool into blocks. From these blocks, 5um sections were cut and mounted on charged glass slides, baked overnight at 60°C and passed through Xylene, graded ethanol, and double distilled water to remove paraffin and rehydrate tissue sections. A Leica Autostainer XL was used to complete the deparaffinization, rehydration and routine hematoxylin and eosin stain preparing the slides for examination by a board-certified veterinary pathologist using HALO software (Indica Labs, Albuquerque, NM).

For IHC staining, tissue sections were mounted on Superfrost Plus Microscope slides (Fisher Scientific, Carlsbad, CA), incubated for 1 hour at 60°C, and passed through Xylene, graded ethanol, and double distilled water to remove paraffin and rehydrate tissue sections. A microwave was used for heat induced epitope retrieval (HIER). Slides were boiled for 20 minutes in a Tris based solution, pH 9 (Vector Laboratories, Burlingame, CA), supplemented with 0.01% Tween-20. Slides were briefly rinsed in hot, distilled water and transferred to a hot citrate based solution, pH 6.0 (Vector Laboratories, Burlingame, CA) where they were allowed to cool to room temperature. All slide manipulation from this point forward was done at room temperature with incubations taking place in a black humidifying chamber. Once cool, slides were rinsed in tris buffered saline (TBS) and incubated with Background Punisher (Biocare Medical, Pacheco, CA) for 10 minutes. Slides were then submerged in a solution of TBS supplemented with 0.01% TritonX100 (TBS-TX100) and placed on a rocker platform for two 5 minute washes followed by a TBS rinse before being returned to humidifying chamber to be incubated with serum free protein block (Dako, Santa Clara, CA) for 20 minutes. Mouse anti-Granzyme primary antibody (Table S6) was then added to the slides and allowed to bind for 60 minutes. Slides were then washed twice with TBS-TX100 and once with TBS. The labeling of the antibody for visualization was done using the MACH3 AP kit (Biocare Medical, Pacheco, CA). Both the MACH3 probe and polymer were incubated for 20 minutes with TBS-TX100 and TBS washes in between. Slides were incubated with permanent red substrate (Dako, Santa Clara, CA) for 20 minutes and placed in TBS to halt the enzymatic reaction.

All other staining was done consecutively with the following method. Slides were incubated with a blocking buffer comprised of 10% normal goat serum (NGS) and 0.02% fish skin gelatin in phosphate buffered saline (PBS) for 40 minutes. This blocking buffer

was also used to dilute both primary and secondary antibodies (Table S6). Primary antibodies were added to slides for 60 minutes. After washing two times with PBS supplemented with 0.02% fish skin gelatin and 0.01% TritonX100 (PBS-FSG-TX100) and once with PBS-FSG, slides were incubated for 40 minutes with a secondary antibody made in goat, raised against the primary host species, and tagged with an Alexa Fluor fluorochrome (488 or 568). The 3 washes mentioned above were repeated before DAPI nuclear stain was added for 10 minutes. Slides were mounted using anti-quenching mounting media containing Mowiol (Sigma, St Louis, MO) and DABCO (Sigma, St Louis, MO) and allowed to dry overnight before imaging with a Axio Slide Scanner (Zeiss, Hamburg, Germany). HALO software (Indica Labs Albuquerque, NM) was used for quantification and analysis.

Detection of Neutralizing Antibodies in Serum

Pseudovirus neutralization testing of serum samples was performed using a SARS-CoV-2.D614G spike-pseudotyped virus in 293/ACE2 cells, with neutralization assessed via reduction in luciferase activity as described[24,25].

Statistical Analysis

GraphPad Prism (version 9 GraphPad Software, LaJolla California) was used for all graphing and statistical analyses. The Kruskal-Wallis with Dunn's multiple comparison test was used to compare changes in cell frequencies and surface marker, cytokine and Granzyme B expression,

Results

Viral dynamics

Four pigtail macaques (PTM) inoculated with SARS-CoV-2 were followed via blood, mucosal swab and bronchoalveolar lavage (BAL) sampling. Two animals were euthanized at 6 days post infection (dpi) and two at 21 dpi (Figure 1A). Quantitative RT-PCR was used to track viral genomic and subgenomic RNA through the course of the study at several sites. We detected both genomic and subgenomic SARS-CoV-2 RNA in all four animals throughout the first several days of infection (Figure 1B-K). One animal, MA27, euthanized at 6-days post infection (dpi), showed a spike in genomic and subgenomic viral RNA (vRNA) at necropsy in the pharynx (Figure 1D,E), with viral levels also beginning to rise in the nasal cavity (Figure 1B,C). MA28, euthanized at 21-dpi, showed detectable levels of vRNA in the nasal and rectal mucosa throughout the course of the study (Figure 1B,J). These findings are consistent with viral kinetics seen in Rhesus macaques with the possible exception of lower viral loads in the pharynx in the PTM model.

Pulmonary disease and pathology

Thoracic radiographs were obtained from all animals before infection and weekly after, revealing subtle changes consistent with interstitial pneumonia reflective of mild to moderate COVID-19 (Figure S1A-L). Postmortem examination at 6-days post infection (dpi) revealed mild-to-moderate SARS-CoV-2-associated pneumonia in one of the two animals, MA27. The pneumonia was characterized by multifocal tan-plum areas of consolidation in the caudal left lung lobe (Figure S2A, Table S1). At 21-dpi, gross lesions were minimal and only observed in one of two animals, MA28. The lesions in this animal were two small, flat tan foci on the dorsolateral aspect of the left caudal lung lobe (Figure S2D, Table S1).

Histopathological findings consistent with SARS-CoV-2 associated pneumonia were observed in both animals at 6-dpi. Both animals had an interstitial pneumonia that was localized to regions of the left caudal lung. Regions of interstitial pneumonia were characterized by alveolar septa that were mild to markedly expanded by a mixture of macrophages, lymphocytes, and neutrophils. Alveolar septa were frequently lined by type II pneumocytes (Figure 2C&D), and alveoli contained large numbers of alveolar macrophages with rafts of fibrin in more severely affected areas (Figure 2A-D).

At 21-dpi, minimal-to-mild residual interstitial pulmonary inflammation was observed in both animals. The residual inflammation was composed of perivascular lymphoid aggregates along with mild thickening of alveolar septa (Figure 2E&F). The inflammatory infiltrate at this time point was composed predominately of lymphocytes; however, in one animal, MA28, low numbers of multinucleated giant cells were present in alveoli. (Figure 2H).

Serum cytokine measures of inflammation

We next measured a panel of cytokines in blood serum after infection. Fluctuations in several inflammatory cytokine levels, as compared to baseline, were found throughout the study. Interleukin-8 (IL-8), a neutrophil chemoattractant, was the most consistently increased cytokine at 6-dpi whereas IL-6 and IL-12-p40 decreased in all animals at day 6 (Figure 3A). Interestingly, MA27 had a stronger inflammatory cytokine response at 6-dpi compared to the other three animals, as exemplified by increases in several cytokines, including IL-10, IFN-γ, GM-CSF, IL-8, IL-17A, MCP-1 and most notably, TNF-α and IFN-β. As stated previously, this animal had increasing viral loads at 6-dpi suggesting a possible link between the intensity of the inflammatory response and the level of replicating virus. Animal MA28, which exhibited consistently high genomic vRNA

levels in both nasal and rectal swabs through 21-dpi, showed a rise IL-10, IL-1β, IL-12p40 and IP-10 serum levels at necropsy (21-dpi).

Markers of coagulopathy

Complications related to coagulopathy have been reported in humans with severe COVID-19 disease, with highly elevated levels of D-dimers in particular a biomarker of disease severity[26,27]. To examine whether PTM recapitulate this phenotype, we measured multiple biomarkers of coagulation in blood (Figure 3B), including fibrinogen, prothrombin, factor XIII, antithrombin, plasminogen, and D-dimers. We found nearly universal increases in coagulation biomarkers in the first week of infection. Specifically, we noted increased D-dimer levels in all four animals at 6-dpi, with MA27 and MA28 exhibiting a greater than 3-fold increase relative to baseline before resolving to near baseline levels. Interestingly, several biomarkers (fibrinogen, prothrombin, factor XIII, antithrombin, and plasminogen) began to rise again at 21-dpi.

Kynurenine tryptophan pathway

Pro-inflammatory cytokines, specifically interferon gamma-**γ** (IFN-**γ**), promote the kynurenine (Kyn) pathway (KP) of tryptophan (Trp) catabolism[28]. Recent studies in humans hospitalized with COVID-19 suggest that the Kyn:Trp ratio positively correlates with disease severity[29]. We measured the Kyn:Trp ratio in plasma at baseline, and days 6, 14 and 21 (Figure 3C, S3A,B). Again, MA27 showed the greatest increase in the Kyn:Trp ratio at 6-dpi possibly providing another biomarker of the more severe disease course seen in this animal.

NK cells

The initial immune response to SARS-CoV-2 infection involves the intricate interplay between cells of the innate immune system. Natural killer (NK) cells are cytotoxic lymphocytes that often play a key role in the early defense against viral infections. Studies of hospitalized COVID-19 patients show that decreases in circulating NK cells correlate with disease severity[30,31]. Here, we measured the percentage of NK cells (defined as CD45+ CD3- CD8+) in both the blood and bronchoalveolar lavage fluid (BAL) at baseline, and days 6-, 14-, and 21-post infection (Figure 3D&E). We did not find significant changes in NK cells in our study. However, MA28 and MA24 had slight increases in circulating NK cells at day 6 and day 14, respectively. Flow cytometry analysis of BAL indicated an increase in infiltrating NK cells in the lung at 6-dpi in all four animals.

Neutrophil to lymphocyte ratio

A high incidence of neutrophilia coupled with lymphocytopenia has been reported in COVID-19 patients[31,32]. Animals MA24, MA27, and MA28 all experienced neutrophilia and lymphocytopenia during the course of the study but the changes were mild and values largely stayed within normal limits. Pre-infection data on these cells were not available for MA30 (Table S1). The neutrophil to lymphocyte ratio (NLR) has been identified as an important predictor of disease severity in human patients[33]. We thus measured the NLR at baseline and 6-, 14- and 21-dpi. MA27 had the highest NLR at 1- and 4-days post infection (Figure 3F-H). These data are consistent with the increased inflammatory cytokine and D-dimer levels, higher K:T ratio, and increasing viral titers at the time of necropsy observed in MA27. Each potentially correlate with or contribute to the more severe lung pathology observed in this animal at necropsy.

SARS-CoV-2 infection and macrophage pulmonary infiltration

Fluorescent immunohistochemistry of the lung for SARS-CoV-2 nucleoprotein identified small clusters of SARS-CoV-2 infected cells, predominately lining the alveolar septa, in both animals sacrificed at 6-dpi (Figure 4 A,B&E). COVID-19 disease is commonly characterized by pulmonary infiltration of inflammatory immune cells[34]. Innate cells, particularly monocytes/macrophages are considered important mediators of disease progression[35]. At 6-dpi, the alveoli contained large numbers of IBA1+ macrophages (Figures 4A-D,F). By 21-dpi, macrophage numbers were greatly reduced and no SARS-CoV-2+ cells were detected in either MA24 or MA28 (Figure 4C-F).

Flow cytometry showed increases in CD14+ CD16- classical monocytes in both the blood and BAL at 6-dpi (Figures 4I&L) and an increase in CD14+ CD16+ intermediate monocytes (Figure 4M) in BAL at 6-dpi. Heterogeneous fluctuations of circulating intermediate and CD14- CD16+ non-classical monocytes occurred throughout the study (Figures 4J&K). MA27 and MA24 showed increases in inflammatory cytokine, tumor necrosis factor-α (TNF-α)-expressing classical monocytes in the BAL at 6-dpi (Figure 4H). Interleukin-1β (IL-1β) and IL-6 are key inflammatory cytokines involved in the pathophysiology of COVID-19 disease in humans[36,37]. Here, we noted increases in IL-1β expression in peripheral CD14+ CD16- monocytes throughout the study (Figure 5A). As indicated in Figure 3A, serum levels of IL-6 remained low after infection. We also found that peripheral monocyte expression of IL-6 stayed relatively stable post infection, with only one animal, MA24, showing an increase at days 14 and 21 compared to 6-dpi (Figure 5B). There was an upward trend that was not statistically significant in neutrophil chemoattractant, IL-8, expression (Figure 5C).

Peripheral T cell responses

Understanding the role of the adaptive immune response to SARS-CoV-2 infection is a key component to the development of effective vaccines and treatment options for

COVID-19. Using flow cytometry, we measured changes to T cell populations in both the blood and BAL at baseline and 6-, 14-, and 21-dpi. CD3+ T cell fluctuations in the blood were driven by CD4 T cells which showed levels increasing significantly between days 14- and 21-pi (Figure 6A). As the percentage of CD4 T cells rise and fall over the course of the study, we observed the opposite pattern in the percentage of cytotoxic CD8 T cells (Figure 6B). We found increases in Ki-67+ CD4 T cells at 6-dpi (MA27, MA28 and MA30) and 14-dpi (MA24 and MA28) indicating increased CD4 T cell proliferation (Figure 6C&D). Increases in expression of the T cell exhaustion marker, PD-1, have been noted in a number of studies involving human COVID-19 patients[38–40]. Here we found a significant increase in PD-1+ CD4 T cells at 14-dpi (Figure 6I). Interestingly, we saw a decrease in the percentage of CD4 T cells at this same timepoint.

We next used tSNE analysis to show changes in PD-1 expressing cell populations over the course of the study (Figures 6E,F,H). At baseline, CD4- CD8- (double negative) T cells made up the greatest proportion of PD-1+ CD3+ T cells (Figure 6H). Beginning at day 6-pi, CD4 T cells made up the majority of PD-1 expressing cells, with only one animal, MA28, showing increases in PD-1 expressing cytotoxic T cells at 6 and 14-dpi (Figure 6J).

Pulmonary T cell responses

We next sought to characterize the dynamics of pulmonary T cell populations over the course of infection by examining the frequency as well as cytokine and surface protein expression before SARS-CoV-2 infection, and at days 6-, 14-, and 21- post viral challenge. Using PMA stimulation, we noted increased frequencies of CD4+/CD8+ double positive (DP) T cells after viral challenge which remained elevated throughout the study (Figure 7A&B) ((Median DP T cells as a percentage of CD3+ T cells: Baseline: 2%

(n=2), 6-dpi: 23% (n=4), 14-dpi: 30% (n=2), 21-dpi: 31% (n=2)). We also examined fold changes in surface protein and cytokine expression among the DP, CD4 and CD8 single positive T cell populations as compared to baseline in two of the animals, MA24 and MA27 (Figure 7E-J). Both MA24 (euthanized at 21-dpi) and MA27 (euthanized at 6-dpi) showed large increases among all three T cell populations in TNF-α expression at 6-dpi. At fourteen days post infection, MA24 showed increased expression of Granzyme B in both the DP and CD8 T cell populations. Interestingly, it was the DP T cell population which showed the greatest fold increase in Granzyme B over baseline indicating the cytotoxic potential of this DP T cell population.

We also compared the activity of each T cell subtype within the same time point of infection (Figure 8A-O). Prior to infection, DP T cells showed higher TNF-α, IFN-$\boldsymbol{\gamma}$, IL-10, MIP-1β, and IL-22 expression than traditional CD4 and CD8 T cells, indicating that these cells may potentially perform a non-specific function in the pulmonary immune response[41]. After viral challenge, we found higher frequencies of Granzyme B expressing DP T cells compared to CD4 T cells and, most notably, CD8 T cells at each timepoint post infection (Figure 8E,J&O). We found significant increases in CD4 T cells expressing IL-2, IL-10 and MIP-1b (Figure 8A-E). At 14-dpi, we noted a significant increase in MIP-1β expressing CD8 T cells (Figure 8I). DP T cells also showed increased activity post viral challenge with significant increases in the frequency of IL-10, TNF-α, MIP-1β and Granzyme B expressing cells. Taken together, these findings show that the DP T cell population has functions which overlap with both CD4 and CD8 T cells[41]. We speculate that these cells are major histocompatibility complex class II (MHC-II) restricted CD4 T cells which upregulate CD8 upon activation, generating the described DP T cell population which has greater cytotoxic potential than traditional CD4

T cells. Pulmonary infiltrating cytotoxic CD4 T cells potentially aid CD8 T cells in viral clearance and are a unique aspect of COVID-19 disease[21].

CD4 T cell and Granzyme B expression in the lungs

Fluorescent Immunohistochemistry (IHC) identified cytotoxic CD4 T cells (CD4+ Granzyme B+) in the lungs of all four PTM at necropsy (Figure 9). We detected large numbers of infiltrating Granzyme B positive cells in the lungs of MA27 and MA30 (euthanized at 6-dpi) along with rare cytotoxic T cells (Figure 9A,B,F,G). At 21-dpi, MA24 (Figure 9C) showed low numbers of Granzyme B+ cells compared to MA28 (Figure 9D) and the other two animals which were euthanized at 6-dpi. Cytotoxic CD4 T cells were detected in the lung of MA28 and, with less frequency, in MA24 (Figure 9G).

We then used flow cytometry to measure cytotoxic CD4 T cells in BAL (CD45+CD3+CD4+Granzyme B+). To mirror the IHC analysis, we did not exclude CD8+ cells from our cytotoxic CD4+ population. Mononuclear cells were stimulated with PMA cocktail and cytotoxic CD4 T cells were measured as a percentage of CD45+ cells (Figure 9H&J) and CD3+ T cells (Figure 5I&K) in both the stimulated and unstimulated conditions. We noted a considerable increase in cytotoxic CD4 T cells in BAL at 14-dpi.

SARS-CoV-2 peptide specific T cell response in the lung 21-days post infection

Mononuclear cells, isolated from BAL, were incubated overnight with SARS-CoV-2 peptides and analyzed by flow cytometry. We detected specific CD4 T cell responses against SARS-CoV-2 that localized to the lung 21 days after viral infection. Specifically, we identified CD4 T cell responses to membrane, nucleocapsid and to a lesser degree, spike peptides (Figure 10A). CD8 T cell responses against the virus were also noted, but at lower frequencies (Figure 10B). In FlowJo, we gated on the CD4 T cell population and

applied tSNE analysis to identify and characterize virus specific CD4 T cells responding to membrane and nucleocapsid viral peptides (Figure 10C&D). tSNE analysis revealed a unique cluster of CD4 T cells that responded to stimulation. In this population of responding cells (Figure 10E&F), we noted increased expression of CD8 and HLA-DR, indicating cell activation. Increased expression of inflammatory cytokines and chemokines was also detected in the antiviral CD4 T cells. We noted a decrease in Granzyme B expression suggesting that the antigen specific CD4 T cells have reduced cytotoxic capacity, unlike the DP T cells (cytotoxic CD4) described previously (Figures 7, 8 and 9). As expected, antiviral CD4s have increased CD95 expression indicating a memory phenotype. Numerous studies of SARS-CoV-2 convalescent humans have described antiviral T cells with a relative predominance of CD4 T cells[42,43]. These antiviral responses are most often noted in the blood. In our study, we were unable to detect antigen-specific T cell responses in the blood 21 days after viral infection (data not shown). Taken together, our data provide a valuable addition to the data from humans and may suggest important roles for antiviral CD4 T cells in the pulmonary compartment.

Humoral immune responses

Using flow cytometry, we measured B cell kinetics in the blood at baseline and days 6-, 14- and 21-post infection (Figure 11A). We did not detect any significant changes in the percentage of peripheral B cells over the course of the study. We next tested serum from infected animals for neutralizing antibodies using a pseudovirus assay. Not surprisingly, no neutralization was detected at 6-dpi in any sample, including the animals euthanized at that time point. By 14-dpi, neutralizing antibody responses were detectable in both MA24 and MA28 with responses decreasing by 21-dpi (Figure 11B).

Discussion

The novel coronavirus SARS-CoV-2 has caused a global pandemic with little precedent. As of the time of submission, this virus has infected nearly 190 million individuals worldwide and killed four million, including over 600,000 in the United States. Illness caused by this virus, termed COVID-19, ranges from asymptomatic[44,45] to flu-like symptoms to severe pneumonia[46,47]. In the most severe cases, patients have experienced acute respiratory distress syndrome (ARDS) and death[48]. It has also become apparent that a number of surprising symptoms can be associated with SARS-CoV-2 infection, including: coagulopathy, thrombosis, kidney failure and chronic respiratory/neurological issues that seemingly persist well beyond viral clearance[36,49–56]. Although several highly effective vaccines have been created to combat the COVID-19 pandemic[57–59], billions of individuals remain unvaccinated worldwide. Furthermore, the emergence of new viral variants with enhanced transmissibility[60–63] and the ability to infect even the vaccinated[64] (though this population is overwhelmingly protected from severe disease[65–67]) suggest that this virus will persist indefinitely. Barring the development and mass deployment of vaccines capable of inducing sterilizing immunity, an exceedingly difficult task, intense research focus must remain to decipher disease mechanisms so those that do become infected can be treated.

Critical to both understanding and treating the broad spectrum of disease sequelae caused by SARS-CoV-2 is the development of animal models that faithfully recapitulate COVID-19. Animal models allow timed infection and euthanasia along with extensive sample collection that are not possible during human infections. Rhesus macaques (RhM), cynomolgus macaques (CyM), and African green monkeys (AGM) have all been used to achieve this goal[12–15,68]. To date, none of these models consistently recapitulate severe COVID-19 disease but some data suggest AGM may exhibit more severe

disease than the others[12,13]. When infected with simian immunodeficiency virus (SIV), pigtail macaques (PTM) exhibit rapid and severe disease relative to RhM and CyM, including rapid destruction of the CD4 immune compartment, severe gastrointestinal disease, and complications related to coagulopathy[17–19,69–71]. Many of these disease features are also relevant to severe COVID-19 disease[49–54,72–74]. A recent report demonstrated that a related species of pigtail macaques showed an abbreviated period of SARS-CoV-2 viral replication but possibly more severe disease than RhM[75]. Thus, PTM may be a reasonable model for severe disease and used to test novel therapeutics and vaccines to prevent disease.

We infected a small cohort of PTM with SARS-CoV-2 through a combination of intratracheal and intranasal instillation. Animals were tracked for viral replication in multiple sites, for immune dynamics in blood and bronchoalveolar lavage cells, and for innate and other markers of disease in blood and tissues. We identified a range of disease severity, even in our small cohort, with one animal euthanized at six days post infection showing more severe pulmonary lesions than the rest. Interestingly, multiple early indicators that are consistent with a more severe disease course in humans, were also detected in this animal, including: viral titer, an elevated neutrophil to lymphocyte ratio, elevated kynurenine to tryptophan ratio, and elevated serum inflammatory cytokines. Our findings suggest that these factors correlate with and may predict disease severity. Expanded cohort sizes that include both male and females as well as aged animals may uncover additional clinical manifestations.

Viral dynamics were similar in PTM as we have reported in RhM[12,13]. Viral RNA, including subgenomic RNA, was consistently detected throughout the first several days of infection. We detected persistent viral titers at multiple sites in some of the animals

throughout the course of the study. These data confirm PTM as a robust model of viral infection and replication, similar to RhM, and suggest this model may be used to study novel virus host relationships.

COVID-19 disease is commonly characterized by pulmonary infiltration of inflammatory immune cells[34]. Innate cells, particularly monocytes, are considered important mediators of disease progression[35]. Although infiltrating monocytes were identified in our PTM, T cells were a more dominant cellular infiltrate into lungs as detected in bronchoalveolar lavage sampling. Specifically, we identified a unique population of CD4+/CD8+ double positive T cells that upregulated inflammatory cytokines such as TNF-α as well as Granzyme B over the course of infection. Traditionally, these cells would be predicted to be major histocompatibility complex class II (MHC-II) restricted CD4 T cells that upregulate CD8 upon activation. Pulmonary infiltrating CD4 T cells with cytotoxic capacity, as measured by Granzyme B, are a unique and possibly understudied aspect of COVID-19 disease.

We also identified relatively high magnitude CD4 T cell responses against the virus that localized to the lung 21 days after viral infection. CD8 T cells against the virus were also noted, but at lower frequencies. Many studies have reported antiviral T cells in SARS-CoV-2 convalescent humans, with a relative predominance of CD4 T cells, however these responses are nearly always noted in blood[42,43]. Thus, our data provide a valuable addition to the data from humans and may suggest important roles for antiviral CD4 T cells in pulmonary sites.

Taken together, our data define a new animal model for COVID-19. PTM show robust viral replication, SARS-CoV-2 associated pneumonia, and complex innate and adaptive

immune responses that may shed light on mechanisms of COVID-19 disease. This model may prove valuable for testing novel immunomodulatory therapeutics and vaccines, including those that modulate pulmonary infiltration of T cells and other inflammatory cells. Finally, our data confirmed COVID-19 associated inflammation was not always resolved 21dpi, despite no evidence of continued viral replication at that time point. Thus, this model may also be valuable for the study of long-term chronic effects associated with SARS-CoV-2 infection.

Figure legends

Figure 1. Viral dynamics. A. Outline of study design. Four PTM were exposed to 1x10^6 TCID50 of SARS-CoV-2 (isolate WA1/2020) through a combination of intranasal and intratracheal inoculation on Day 0. Figure created with BioRender.com. **B-K**. Quantification of SARS-CoV-2 RNA levels from mucosal swabs overtime (Quantitative RT PCR). Genomic (**B,D,F,H,J**) Subgenomic (**C,E,G,I,K**). B-K Baseline: n=4, Day 1: n=4, Day 4: n=4, Day 6: n=4, Day 14: n=2, Day 21: n=2

Figure 2. Histopathologic findings in SARS-CoV-2 infected pigtail macaques (PTM). Histopathologic findings at 6- **(A-D)** and 21-dpi **(E-H)**. **A&B.** At 6-dpi alveolar septa are expanded by inflammatory infiltrate and alveoli contain rafts of fibrin (**arrows**). **C&D.** The inflammatory infiltrate is composed of a mixture of histiocytes, lymphocytes, and neutrophils, and alveolar septa are frequently lined by type II pneumocytes (**arrows**). In severely affected areas, alveoli contain fibrin rafts (**C, asterisks**). **E&F.** At 21-dpi, there is residual inflammation composed of perivascular lymphoid aggregates (**asterisks**), and mild thickening of alveolar septa (**arrows). G&H**. The residual inflammation is composed predominately of lymphocytes, and in MA28, rare multinucleated giant cells (**H, arrows**).

Figure 3. Inflammatory innate immune response in pigtail macaques challenged with SARS-CoV-2. A. Changes in serum cytokine levels at 6-, 14- and 21-days post SARS-CoV-2 infection. Data represent fold changes from baseline. **B.** Changes in coagulation biomarkers in plasma at 4-, 6-, 14- and 21-days post infection (dpi). Data are fold changes from baseline. **C.** Ratio of Kynurenine (Kyn) to Tryptophan (Trp) as a measure of indoleamine 2,3-dioxygenase (IDO) activity before and after SARS-CoV-2 infection. **D&E.** Frequency of Natural Killer (NK, CD45+ CD3- CD8+) cells in the blood (**D**) or **(E)** BAL at baseline, 6-, 14- and 21-days post infection (dpi). Bars represent median **F.** Absolute number of neutrophils pre- and post- SARS-CoV-2 infection. **G.** Absolute number of lymphocytes pre- and post-SARS-CoV-2 infection. **H.** Changes in neutrophil to lymphocyte ratio before and after SARS-CoV-2 infection. Figures 3C&D Baseline: n=4, Day 6: n=4, Day 14: n=2, Day 21: n=2; Figure 3E Baseline: n=3, Day 6: n=4, Day 14: n=2, Day 21: n=2; Figures 3F-H Baseline: n=3, Day 1: n=4, Day 4: n=4 Day 6: n=4, Day 14: n=2, Day 21: n=2. Figures C-H Day 0=day of infection. Kruskal-Wallis test for variance for overall medians used to determine significance. Kruskal-Wallis comparison of overall means (P_{KW}) test used to determine significance. P values ≤0.05 reported

Figure 4. Pulmonary SARS-CoV-2 infection and macrophage/monocytes in the lung and blood. A-D. SARS-CoV-2 infection and macrophage infiltration in the lungs of pigtailed macaques at 6- (**A&B**) and 21- days post infection (dpi, **C&D**). DAPI=White, Green=SARS-CoV-2, Red=IBA1,Blue=Autofluorescence. **E-F.** Percentage of SARS-CoV-2 infected cells (**E**) and IBA1+ macrophages (**F**) in the lung at necropsy. Bars represent median. **G&H**. Frequency of IL-8 (**G**) and TNF-α (**H**) expressing classical monocytes (CD45+ HLA-DR+ CD14- CD16+) in BAL. **I-O.** Classical (**I&L**) intermediate

(CD45+ HLA-DR+ CD14+ CD16+) (**J&M**), and non-classical monocytes (CD45+ HLA-DR+ CD14- CD16+) (**K&O**) frequencies in the blood and BAL before and after SARS-CoV-2 infection. Day 0=day of infection. I-O Baseline (day -7): n=3, Day 6: n=4, Day 14: n=2, Day 21: n=2. Kruskal-Wallis comparison of overall means (P_{KW}) and Dunn's Multiple comparisons (designated by line, P_D) tests used to determine significance. P values ≤0.05 reported

Figure 5. A-D. Monocyte cytokine response in the blood of pigtail macaques challenged with SARS-CoV-2. Frequency of IL-1β (**A**), IL-6 (**B**), IL-8 (**C**) and TNF-α (**D**) expressing classical monocytes (CD45+ HLA-DR+ CD14- CD16+) in the blood. Bars represent median. Day 0=day of infection. Baseline (-7): n=3, Day 6: n=4, Day 14: n=2, Day 21: n=2.

Figure 6. T cells in the blood. **A-B.** CD4+ (**A**) and CD8+ (**B**) T cell frequencies in the blood before and 1-, 2-, and 3-weeks post SARS-CoV-2 infection. **C-D.** Changes in Ki-67 expressing CD4+ (**C**) and CD8+ (**D**) T cells. Bars represent median **E.** tSNE plots displaying changes in PD-1 expression (red) in peripheral CD45+ cells overtime. MA24 (**E**) and MA28 (**F**) displayed as a representative animal. **G.** Merged tSNE indicating phenotype of the tSNE defined cell populations in E. **H.** Average changes in the percentages of CD4+, CD8+, CD4- CD8- (DN) and CD4+ CD8+ (DP) T cells within the total PD-1+ CD3+ cell population. **I-L.** Frequency of PD-1+ expressing CD4+ (**I**), CD8+ (**J**), DP (**K**) and DN (**L**) T cells in the blood. Bars represent median. Kruskal-Wallis comparison of overall means (P_{KW}) and Dunn's Multiple comparisons (designated by line, P_D) tests used to determine significance. P values ≤0.05 reported. Baseline (-7): n=4, Day 6: n=4, Day 14: n=2, Day 21: n=2.

Figure 7. Adaptive T cell responses in the BAL. **A.** Representative flow cytometry plots showing changes in CD4 and CD8 expression in PMA/ionomycin stimulated CD3+ cells in BAL. Two animals shown (MA24 necropsied at 21-dpi, MA27 necropsied at 6-dpi). **B-D.** Effect of PMA/ionomycin on the frequency of CD4+ CD8+ (DP, **B**) CD4+ (**C**) and CD8+ (**D**) T cells in BAL before and 6-, 14-, and 21-days post SARS-CoV-2 infection. Bars represent mean and standard deviation. **E-J.** Nightingale Rose Plots (NRPs) showing fold changes in cytokine and surface protein expression compared to baseline (MFI). Yellow=6-dpi, Purple=14-dpi, Green=21-dpi. Size of petals represents magnitude of increase in expression. Distance from one white ring to the next is a 1-fold change. A decrease in expression is represented by a petal size less than the distance between two rings. Two animals shown (MA24 necropsied at 21-dpi, MA27 necropsied at 6-dpi). At 6-dpi, MA24 DP T cell TNF-α MFI is 24x baseline and CD4+ T cell TNF-α MFI is 50x baseline. Graph cutoff is set to a 12-fold change. **B-D.** Baseline: n=3 (No Stimulation (Stim)) and n=2 (Stim), Day 6: n=4 (No Stim) and n=4 (Stim), Day 14: n=2 (No Stim) and n=2 (Stim), Day 21: n=2 (No Stim) and n=2 (Stim).

Figure 8. Changes in T cell cytokine expression in the lung. A-O. PMA/ionomycin stimulated CD4+ T cells (**A-E**), CD8+ T cells (**F-J**), and CD4+ CD8+ (DP) T cells (**K-O**). Bars represent median. Kruskal-Wallis comparison of overall means (P_{KW}) and Dunn's Multiple comparisons (designated by line, P_D) tests used to determine significance. P values ≤0.05 reported. Baseline (-7): n=2, Day 6: n=4, Day 14: n=2, Day 21: n=2.

Figure 9. CD4 and Granzyme B expression in the lungs of SARS-CoV-2 infected macaques at 6- (A&B) and 21-days post infection (dpi, C&D). At 6-dpi, MA27 (**A**) and MA30 (**B**) the lungs are infiltrated by large numbers of Granzyme B positive cells (red, arrows). Insets: Rare CD4+ cells (green) exhibit granzyme expression. At 21-dpi, MA24

(**C**) exhibits low numbers of Granzyme B positive cells (red, arrows) compared to MA28 (**D**) and the two, 6-dpi animals (**A&B**). DAPI=Blue, Green=CD4, Red=Granzyme B. **E-G.** Percentage of CD4+ (**E**), Granzyme B+ (**F**) and CD4+ Granzyme B+ (**G**) cells in the lung at necropsy. Bars represent median. **H-K.** CD4+ Granzyme B+ T cells (CD45+ CD3+ CD4+ Granzyme B+) in BAL at Baseline (-7) and 6-, 14- and 21-dpi as a percentage of CD45+ cells (**H&J**) and CD3+ cells (**I&K**). **H&I**. Mononuclear cells, isolated from BAL, were stimulated with PMA/ionomycin for 4-6 hours. Bars represent median and standard deviation. Kruskal-Wallis comparison of overall means (P_{KW}) and Dunn's Multiple comparisons (designated by line, P_D) tests used to determine significance. P values ≤0.05 reported. **H-K**. Baseline: n=3 (No Stimulation (Stim)) and n=2 (Stim), Day 6: n=4 (No Stim) and n=4 (Stim), Day 14: n=2 (No Stim) and n=2 (Stim), Day 21: n=2 (No Stim) and n=2 (Stim).

Figure 10. SARS-CoV-2 peptide specific T cell response in the lung 21-days post infection. Two animals shown (MA24 & MA28 necropsied 21-dpi) **A&B.** Flow cytometry dot plots showing CD4+ (**A**) and CD8+ (**B**) T cell Interferon-γ (IFN-γ) response to overnight SARS-CoV-2 peptide (spike, membrane, nucleocapsid and envelope) stimulation. No stim o/n=cells incubated overnight without stimulation. Heatmap represents arcsin transformed MFI values. **C&D.** tSNE plots of CD4+ T cells showing an expansion in cells following overnight peptide stimulation. M=SARS-CoV-2 membrane peptides (**C**), N=SARS-CoV-2 nucleocapsid peptides (**D**). **E&F.** Radial bar plot comparing MFI values of the expanded CD4+ T cell population gated on in **C&D** to the unchanged CD4+ population within the same tSNE plot. Representative animals MA24, MA28 (necropsied at 21-dpi). The higher MFI value is set to 100 and the percent difference is calculated between the higher and lower MFI values. Size of the petals represent this analysis.

Figure 11. Humoral immune response in SARS-CoV-2 infected pigtail macaques. **A.** B cell frequencies in the blood before and 6-, 14-, and 21-days post (dpi) SARS-CoV-2 infection. Bars indicate median. **B.** Pseudovirus neutralization assay showing serum antibody levels against SARS-CoV-2 using HEK 293T/ACE2 cells. Baseline (-7): n=4, Day 6: n=4, Day 14: n=2, Day 21: n=2

Supplemental Figure 1. **Radiographs of pigtail macaques (PTM) challenged with SARS-CoV-2.** MA27 baseline (**A**) and 6-days post infection (dpi) (**B**). MA30 at baseline (**C**) and 6-dpi (**D**). MA24 at baseline (**E**), 6-dpi (**F**), 14-dpi (**G**) and 21-dpi (**H**). MA28 at baseline (**I**), 6-dpi (**J**), 14-dpi (**K**) and 21-dpi (**L**). Baseline for all four PTM was established 3-days prior to infection.

Supplemental Figure 2. Gross pathological pulmonary pathology in SARS-CoV-2 infected pigtail macaques (PTM). A-D. Gross pulmonary pathology at 6- (**A&B**) and 21-days post infection (dpi, **C&D**). **A**. MA27, the left caudal lung lobe has multifocal tan-plum areas of consolidation (arrows). Inset: the consolidation extends to the diaphragmatic and medial surface of the left caudal lung. There is no evidence of gross pathology in MA30 (B) or MA24 (C). **D.** MA28, the laterodorsal aspect of the left caudal lobe contains two small, flat tan foci (arrows). Inset: closer view of tan foci.

Supplemental Figure 3. Changes in IDO activity post SARS-CoV-2 Infection. A. Tryptophan (Trp) and **B.** Kynurenine (Kyn) levels in plasma before and after SARS-CoV-2 infection. Day 0=day of infection, Baseline: n=4, Day 7: n=4, Day 14: n=2, Day 21: n=2. dpi=days post infection.

Supplemental Table 1. Clinical, blood and necropsy observations in pigtail macaques (PTM) challenged with SARS-CoV-2 (n=4). Values in parenthesis represent days post SARS-CoV-2 Infection. Neutrophilia, eosinophilia, basophilia, monocytosis defined as ≥ 2-fold increase over baseline[16]. Lymphocytopenia, monocytopenia, eosinopenia, basopenia defined as a 35% reduction from baseline[16]. CRP: C-reactive protein

Supplemental Table 2. Monocyte Flow Cytometry Panel.

Supplemental Table 3. Phenotype Flow Cytometry Panel.

Supplemental Table 4. T cell Flow Cytometry Panel.

Supplemental Table 5. T cell SARS-CoV-2 Peptide, PMA/Ionomycing Stimulation

Supplemental Table 6. Immunohistochemistry Reagent Panel.

Acknowledgements

The following reagents were obtained through BEI Resources, NIAID, NIH: Peptide arrays NR4219, NR-52402, NR-53822, NR-53822. Funding was provided by NIH NAID grants P51OD01110459, R21 AI150413-01, R01 AI38782-01, and R24 AI120942.

Bibliography

1. Stadler K, Masignani V, Eickmann M, et al. SARS--beginning to understand a new virus. *Nat Rev Microbiol*. 2003;1(3):209-218. doi:10.1038/nrmicro775
2. Boni MF, Lemey P, Jiang X, et al. Evolutionary origins of the SARS-CoV-2 sarbecovirus lineage responsible for the COVID-19 pandemic. *Nat Microbiol*. 2020;5(11):1408-1417. doi:10.1038/s41564-020-0771-4
3. Gorbalenya AE, Baker SC, Baric RS, et al. The species Severe acute respiratory syndrome-related coronavirus: classifying 2019-nCoV and naming it SARS-CoV-2. *Nat Microbiol*. 2020;5(4):536-544. doi:10.1038/s41564-020-0695-z
4. Sayampanathan AA, Heng CS, Pin PH, Pang J, Leong TY, Lee VJ. Infectivity of asymptomatic versus symptomatic COVID-19. *Lancet*. 2021;397(10269):93-94. doi:10.1016/S0140-6736(20)32651-9
5. Teo AKJ, Choudhury Y, Tan IB, et al. Saliva is more sensitive than nasopharyngeal or nasal swabs for diagnosis of asymptomatic and mild COVID-19 infection. *Sci Rep*. 2021;11(1):1-8. doi:10.1038/s41598-021-82787-z
6. Xie C, Li Q, Li L, et al. Association of early inflammation with age and asymptomatic disease in covid-19. *J Inflamm Res*. 2021;14:1207-1216. doi:10.2147/JIR.S304190
7. Zhu J, Ji P, Pang J, et al. Clinical characteristics of 3062 COVID-19 patients: A meta-analysis. *J Med Virol*. 2020;92(10):1902-1914. doi:10.1002/jmv.25884
8. McElvaney OJ, McEvoy NL, McElvaney OF, et al. Characterization of the inflammatory response to severe COVID-19 Illness. *Am J Respir Crit Care Med*. 2020;202(6):812-821. doi:10.1164/rccm.202005-1583OC
9. Zhang R, Liu Y, Zhang B, et al. Coagulopathy is associated with multiple organ damage and prognosis of COVID-19. *EXCLI J*. 2021;20:174-191. doi:10.17179/excli2020-2853

10. Zingaropoli MA, Nijhawan P, Carraro A, et al. Increased sCD163 and sCD14 Plasmatic Levels and Depletion of Peripheral Blood Pro-Inflammatory Monocytes, Myeloid and Plasmacytoid Dendritic Cells in Patients With Severe COVID-19 Pneumonia. *Front Immunol*. 2021;12(February):1-12. doi:10.3389/fimmu.2021.627548

11. Zuo Y, Yalavarthi S, Shi H, et al. Neutrophil extracellular traps in COVID-19. *JCI Insight*. 2020;5(11). doi:10.1172/jci.insight.138999

12. Fahlberg MD, Blair R V., Doyle-Meyers LA, et al. Cellular events of acute, resolving or progressive COVID-19 in SARS-CoV-2 infected non-human primates. *Nat Commun*. 2020;11(1):1-14. doi:10.1038/s41467-020-19967-4

13. Blair R V, Vaccari M, Doyle-Meyers LA, et al. Acute Respiratory Distress in Aged, SARS-CoV-2–Infected African Green Monkeys but Not Rhesus Macaques. *Am J Pathol*. 2021;191(2):274-282. doi:https://doi.org/10.1016/j.ajpath.2020.10.016

14. Munster VJ, Feldmann F, Williamson BN, et al. Respiratory disease in rhesus macaques inoculated with SARS-CoV-2. *Nature*. 2020;585(7824):268-272. doi:10.1038/s41586-020-2324-7

15. Hartman AL, Nambulli S, McMillen CM, et al. SARS-CoV-2 infection of African green monkeys results in mild respiratory disease discernible by PET/CT imaging and shedding of infectious virus from both respiratory and gastrointestinal tracts. *PLoS Pathog*. 2020;16(9):1-24. doi:10.1371/journal.ppat.1008903

16. Woolsey C, Borisevich V, Prasad AN, et al. Establishment of an African green monkey model for COVID-19 and protection against re-infection. *Nat Immunol*. 2021;22(1):86-98. doi:10.1038/s41590-020-00835-8

17. Canary LA, Vinton CL, Morcock DR, et al. Rate of AIDS progression is associated with gastrointestinal dysfunction in simian immunodeficiency virus-infected pigtail macaques. *J Immunol*. 2013;190(6):2959-2965. doi:10.4049/jimmunol.1202319

18. Klatt NR, Canary LA, Vanderford TH, et al. Dynamics of simian immunodeficiency virus SIVmac239 infection in pigtail macaques. *J Virol*. 2012;86(2):1203-1213. doi:10.1128/JVI.06033-11

19. Klatt NR, Harris LD, Vinton CL, et al. Compromised gastrointestinal integrity in pigtail macaques is associated with increased microbial translocation, immune activation, and IL-17 production in the absence of SIV infection. *Mucosal Immunol*. 2010;3(4):387-398. doi:10.1038/mi.2010.14

20. Metcalf Pate KA, Lyons CE, Dorsey JL, et al. Platelet Activation and Platelet-Monocyte Aggregate Formation Contribute to Decreased Platelet Count During Acute Simian Immunodeficiency Virus Infection in Pig-tailed Macaques. *J Infect Dis*. 2013;208(6):874-883. doi:10.1093/infdis/jit278

21. Kaneko N, Boucau J, Kuo H-H, et al. Expansion of Cytotoxic CD4+ T cells in the lungs in severe COVID-19. *medRxiv Prepr Serv Heal Sci*. March 2021. doi:10.1101/2021.03.23.21253885

22. Beddingfield BJ, Maness NJ, Fears AC, et al. Effective prophylaxis of COVID-19 in rhesus macaques using a combination of two parentally-administered SARS-CoV-2 neutralizing antibodies. *bioRxiv*. January 2021:2021.05.26.445878. doi:10.1101/2021.05.26.445878

23. Amir EAD, Davis KL, Tadmor MD, et al. ViSNE enables visualization of high dimensional single-cell data and reveals phenotypic heterogeneity of leukemia. *Nat Biotechnol*. 2013;31(6):545-552. doi:10.1038/nbt.2594

24. Shen X, Tang H, McDanal C, et al. SARS-CoV-2 variant B.1.1.7 is susceptible to neutralizing antibodies elicited by ancestral spike vaccines. *Cell Host Microbe*. 2021;29(4):529-539.e3. doi:10.1016/j.chom.2021.03.002

25. Weissman D, Alameh MG, de Silva T, et al. D614G Spike Mutation Increases SARS CoV-2 Susceptibility to Neutralization. *Cell Host Microbe*. 2021;29(1):23-

31.e4. doi:10.1016/j.chom.2020.11.012

26. Zhou F, Yu T, Du R, et al. Clinical course and risk factors for mortality of adult inpatients with COVID-19 in Wuhan, China: a retrospective cohort study. *Lancet (London, England)*. 2020;395(10229):1054-1062. doi:10.1016/S0140-6736(20)30566-3

27. Yu H-H, Qin C, Chen M, Wang W, Tian D-S. D-dimer level is associated with the severity of COVID-19. *Thromb Res*. 2020;195:219-225. doi:10.1016/j.thromres.2020.07.047

28. Rebnord EW, Strand E, Midttun Ø, et al. The kynurenine:tryptophan ratio as a predictor of incident type 2 diabetes mellitus in individuals with coronary artery disease. *Diabetologia*. 2017;60(9):1712-1721. doi:10.1007/s00125-017-4329-9

29. Lionetto L, Ulivieri M, Capi M, et al. Increased kynurenine-to-tryptophan ratio in the serum of patients infected with SARS-CoV2: An observational cohort study. *Biochim Biophys Acta - Mol Basis Dis*. 2021;1867(3):166042. doi:10.1016/j.bbadis.2020.166042

30. Zheng M, Gao Y, Wang G, et al. Functional exhaustion of antiviral lymphocytes in COVID-19 patients. *Cell Mol Immunol*. 2020;17(5):533-535. doi:10.1038/s41423-020-0402-2

31. Song CY, Xu J, He JQ, Lu YQ. COVID-19 early warning score: A multi-parameter screening tool to identify highly suspected patients. *medRxiv*. 2020. doi:10.1101/2020.03.05.20031906

32. Zhang B, Zhou X, Zhu C, et al. Immune Phenotyping Based on the Neutrophil-to-Lymphocyte Ratio and IgG Level Predicts Disease Severity and Outcome for Patients With COVID-19. *Front Mol Biosci*. 2020;7. doi:10.3389/fmolb.2020.00157

33. Liu J, Liu Y, Xiang P, et al. Neutrophil-to-lymphocyte ratio predicts critical illness patients with 2019 coronavirus disease in the early stage. *J Transl Med*.

2020;18(1):1-12. doi:10.1186/s12967-020-02374-0

34. Mauvais-Jarvis F, Klein SL, Levin ER. Estradiol, Progesterone, Immunomodulation, and COVID-19 Outcomes. *Endocrinol (United States)*. 2020;161(9):1-8. doi:10.1210/endocr/bqaa127

35. Bösmüller H, Matter M, Fend F, Tzankov A. The pulmonary pathology of COVID-19. *Virchows Arch*. 2021;478(1):137-150. doi:10.1007/s00428-021-03053-1

36. Schulte-Schrepping J, Reusch N, Paclik D, et al. Severe COVID-19 Is Marked by a Dysregulated Myeloid Cell Compartment. *Cell*. 2020;182(6):1419-1440.e23. doi:10.1016/j.cell.2020.08.001

37. Hadjadj J, Yatim N, Barnabei L, Corneau A, Boussier J. E (2 , 6 , 7). 2020;724(August):718-724.

38. Diao B, Wang C, Tan Y, et al. Reduction and Functional Exhaustion of T Cells in Patients With Coronavirus Disease 2019 (COVID-19). *Front Immunol*. 2020;11(May):1-7. doi:10.3389/fimmu.2020.00827

39. Bellesi S, Metafuni E, Hohaus S, et al. Increased CD95 (Fas) and PD-1 expression in peripheral blood T lymphocytes in COVID-19 patients. *Br J Haematol*. 2020;191(2):207-211. doi:10.1111/bjh.17034

40. Sattler A, Angermair S, Stockmann H, et al. SARS–CoV-2–specific T cell responses and correlations with COVID-19 patient predisposition. *J Clin Invest*. 2020;130(12):6477-6489. doi:10.1172/JCI140965

41. Diedrich CR, Gideon HP, Rutledge T, et al. CD4CD8 Double Positive T cell responses during Mycobacterium tuberculosis infection in cynomolgus macaques. *J Med Primatol*. 2019;48(2):82-89. doi:10.1111/jmp.12399

42. Meckiff BJ, Ramírez-Suástegui C, Fajardo V, et al. Imbalance of Regulatory and Cytotoxic SARS-CoV-2-Reactive CD4+ T Cells in COVID-19. *Cell*. 2020;183(5):1340-1353.e16. doi:10.1016/j.cell.2020.10.001

43. Weiskopf D, Schmitz KS, Raadsen MP, et al. Phenotype and kinetics of SARS-CoV-2-specific T cells in COVID-19 patients with acute respiratory distress syndrome. *Sci Immunol*. 2020;5(48):1-14. doi:10.1126/SCIIMMUNOL.ABD2071

44. Gandhi M, Yokoe DS, Havlir D V. Asymptomatic Transmission, the Achilles' Heel of Current Strategies to Control Covid-19. *N Engl J Med*. 2020;382(22):2158-2160. doi:10.1056/NEJMe2009758

45. Gatto M, Bertuzzo E, Mari L, et al. Spread and dynamics of the COVID-19 epidemic in Italy: Effects of emergency containment measures. *Proc Natl Acad Sci U S A*. 2020;117(19):10484-10491. doi:10.1073/pnas.2004978117

46. Guan W-J, Ni Z-Y, Hu Y, et al. Clinical Characteristics of Coronavirus Disease 2019 in China. *N Engl J Med*. 2020;382(18):1708-1720. doi:10.1056/NEJMoa2002032

47. Kujawski SA, Wong KK, Collins JP, et al. Clinical and virologic characteristics of the first 12 patients with coronavirus disease 2019 (COVID-19) in the United States. *Nat Med*. 2020;26(6):861-868. doi:10.1038/s41591-020-0877-5

48. Wu JT, Leung K, Bushman M, et al. Estimating clinical severity of COVID-19 from the transmission dynamics in Wuhan, China. *Nat Med*. 2020;26(4):506-510. doi:10.1038/s41591-020-0822-7

49. Fogarty H, Townsend L, Ni Cheallaigh C, et al. COVID19 coagulopathy in Caucasian patients. *Br J Haematol*. 2020;189(6):1044-1049. doi:10.1111/bjh.16749

50. Llitjos J-F, Leclerc M, Chochois C, et al. High incidence of venous thromboembolic events in anticoagulated severe COVID-19 patients. *J Thromb Haemost*. 2020;18(7):1743-1746. doi:10.1111/jth.14869

51. Panigada M, Bottino N, Tagliabue P, et al. Hypercoagulability of COVID-19 patients in intensive care unit: A report of thromboelastography findings and other

parameters of hemostasis. *J Thromb Haemost*. 2020;18(7):1738-1742. doi:https://doi.org/10.1111/jth.14850

52. Porfidia A, Pola R. Venous thromboembolism in COVID-19 patients. *J Thromb Haemost*. 2020;18(6):1516-1517. doi:10.1111/jth.14842

53. Spiezia L, Boscolo A, Poletto F, et al. COVID-19-Related Severe Hypercoagulability in Patients Admitted to Intensive Care Unit for Acute Respiratory Failure. *Thromb Haemost*. 2020;120(6):998-1000. doi:10.1055/s-0040-1710018

54. Klok FA, Kruip MJHA, van der Meer NJM, et al. Incidence of thrombotic complications in critically ill ICU patients with COVID-19. *Thromb Res*. 2020;191:145-147. doi:10.1016/j.thromres.2020.04.013

55. Varga Z, Flammer AJ, Steiger P, et al. Endothelial cell infection and endotheliitis in COVID-19. *Lancet (London, England)*. 2020;395(10234):1417-1418. doi:10.1016/S0140-6736(20)30937-5

56. Bridwell R, Long B, Gottlieb M. Neurologic complications of COVID-19. *Am J Emerg Med*. 2020;38(7):1549.e3-1549.e7. doi:10.1016/j.ajem.2020.05.024

57. Baden LR, El Sahly HM, Essink B, et al. Efficacy and Safety of the mRNA-1273 SARS-CoV-2 Vaccine. *N Engl J Med*. 2021;384(5):403-416. doi:10.1056/NEJMoa2035389

58. Polack FP, Thomas SJ, Kitchin N, et al. Safety and Efficacy of the BNT162b2 mRNA Covid-19 Vaccine. *N Engl J Med*. 2020;383(27):2603-2615. doi:10.1056/NEJMoa2034577

59. Sadoff J, Le Gars M, Shukarev G, et al. Interim Results of a Phase 1-2a Trial of Ad26.COV2.S Covid-19 Vaccine. *N Engl J Med*. 2021;384(19):1824-1835. doi:10.1056/NEJMoa2034201

60. Winger A, Caspari T. The Spike of Concern-The Novel Variants of SARS-CoV-2.

Viruses. 2021;13(6):1002. doi:10.3390/v13061002

61. Singh J, Rahman SA, Ehtesham NZ, Hira S, Hasnain SE. SARS-CoV-2 variants of concern are emerging in India. *Nat Med*. 2021;27(7):1131-1133. doi:10.1038/s41591-021-01397-4

62. Lessells RJ. SARS-CoV-2 variants of concern: the knowns and unknowns. *Anaesthesia, Crit care pain Med*. 2021;40(3):100868. doi:10.1016/j.accpm.2021.100868

63. Walensky RP, Walke HT, Fauci AS. SARS-CoV-2 Variants of Concern in the United States—Challenges and Opportunities. *JAMA*. 2021;325(11):1037-1038. doi:10.1001/jama.2021.2294

64. Olsen RJ, Christensen PA, Long SW, et al. Trajectory of Growth of SARS-CoV-2 Variants in Houston, Texas, January through May 2021 Based on 12,476 Genome Sequences. *Am J Pathol*. July 2021:S0002-9440(21)00317-5. doi:10.1016/j.ajpath.2021.07.002

65. Abu-Raddad LJ, Chemaitelly H, Butt AA, Vaccination NSG for C-19. Effectiveness of the BNT162b2 Covid-19 Vaccine against the B.1.1.7 and B.1.351 Variants. *N Engl J Med*. 2021;385(2):187-189. doi:10.1056/NEJMc2104974

66. Haas EJ, Angulo FJ, McLaughlin JM, et al. Impact and effectiveness of mRNA BNT162b2 vaccine against SARS-CoV-2 infections and COVID-19 cases, hospitalisations, and deaths following a nationwide vaccination campaign in Israel: an observational study using national surveillance data. *Lancet (London, England)*. 2021;397(10287):1819-1829. doi:10.1016/S0140-6736(21)00947-8

67. Wu K, Werner AP, Koch M, et al. Serum Neutralizing Activity Elicited by mRNA-1273 Vaccine. *N Engl J Med*. 2021;384(15):1468-1470. doi:10.1056/NEJMc2102179

68. Woolsey C, Borisevich V, Prasad AN, et al. Establishment of an African green

monkey model for COVID-19 and protection against re-infection. *Nat Immunol*. 2021;22(1):86-98. doi:10.1038/s41590-020-00835-8

69. Pandrea I, Cornell E, Wilson C, et al. Coagulation biomarkers predict disease progression in SIV-infected nonhuman primates. *Blood*. 2012;120(7):1357-1366. doi:10.1182/blood-2012-03-414706

70. Schechter ME, Andrade BB, He T, et al. Inflammatory monocytes expressing tissue factor drive SIV and HIV coagulopathy. *Sci Transl Med*. 2017;9(405):1-14. doi:10.1126/scitranslmed.aam5441

71. Beck SE, Kelly KM, Queen SE, et al. Macaque species susceptibility to simian immunodeficiency virus: increased incidence of SIV central nervous system disease in pigtailed macaques versus rhesus macaques. *J Neurovirol*. 2015;21(2):148-158. doi:10.1007/s13365-015-0313-7

72. Jin X, Lian J-S, Hu J-H, et al. Epidemiological, clinical and virological characteristics of 74 cases of coronavirus-infected disease 2019 (COVID-19) with gastrointestinal symptoms. *Gut*. 2020;69(6):1002 LP - 1009. doi:10.1136/gutjnl-2020-320926

73. Lee I-C, Huo T-I, Huang Y-H. Gastrointestinal and liver manifestations in patients with COVID-19. *J Chin Med Assoc*. 2020;83(6):521-523. doi:10.1097/JCMA.0000000000000319

74. Hunt RH, East JE, Lanas A, et al. COVID-19 and Gastrointestinal Disease: Implications for the Gastroenterologist. *Dig Dis*. 2021;39(2):119-139. doi:10.1159/000512152

75. Song T-Z, Zheng H-Y, Han J-B, et al. Northern pig-tailed macaques (Macaca leonina) infected with SARS-CoV-2 show rapid viral clearance and persistent immune response. *Zool Res*. 2021;42(3):350-353. doi:10.24272/j.issn.2095-8137.2020.334

1

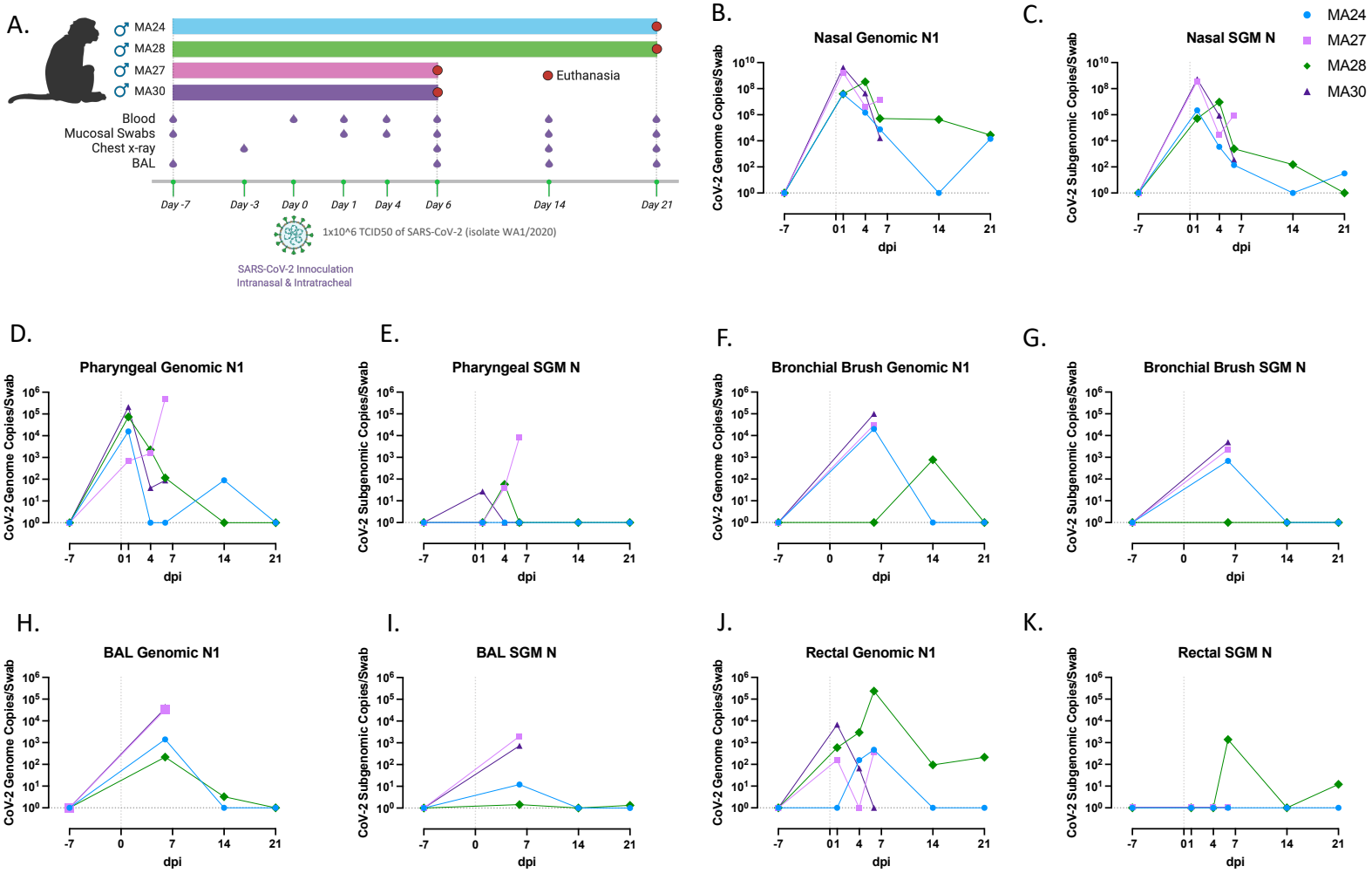

Figure 1. Viral dynamics. A. Outline of study design. Four PTM were exposed to 1x10^6 TCID50 of SARS-CoV-2 (isolate WA1/2020) through a combination of intranasal and intratracheal inoculation on Day 0. Figure created with BioRender.com. **B-K**. Quantification of SARS-CoV-2 RNA levels from mucosal swabs overtime (Quantitative RT PCR). Genomic (**B,D,F,H,J**) Subgenomic (**C,E,G,I,K**). B-K Baseline: n=4, Day 1: n=4, Day 4: n=4, Day 6: n=4, Day 14: n=2, Day 21: n=2

Supplemental Table 1. Clinical, Blood and Necropsy Observations						Necropsy Observations		
Animal ID	**Sex**	**Age (y)**	**Clinical Observations**	**Blood Cell Counts**	**Blood Chemistry**	**Gross Findings**	**Case Summary**	**Other Notes**
MA27	M	6.07	Decreased appetite (5) Soft stool (5) Necropsy 6 dpi	 Neutrophilia (4), Monocytosis (4) Lymphocytopenia (1), Eosinopenia (1, 4) Basopenia (1) Neu/Lym ratio 6.35 (1), 6.26 (4)		Mild subacute pneumonia, lymphoid hyperplasia	Lung lesions in caudal left lobe coincide with gross lesions. Lesions are characterized by mild alveolar epithelial hyperplasia and minimal lymphocytic infiltration. Lymphoid hyperplasia noted in the spleen and all lymph nodes Findings are comparable with lesions in SARS-CoV-2 inocculated Rhesus monkeys	Lungs: caudal left lobe contains two red-grey regions 1 and 2 cm on the lateral aspect and a 3x4 cm zone on the medial aspect. Lymph nodes: Enlarged 3x normal
MA30	M	5.61	Mild cough (2,3) Decreased appetite (1-3, 5) *Had soft stool prior to infection* Necropsy 6 dpi	 No baseline to compare	21-fold ↑ in CRP (1)	Minimal focal subacute pneumonia and lymphoid hyperplasia	Lung lesions are scattered in multiple lobes but are most severe in the caudal left lobe. Lesions consist of extensive alveolar epithelial hyperplasia with lymphocytic infiltration. Lymphoid hyperplasia is noted in the lung, spleen and all lymph nodes Findings are comparable with lesions in SARS-CoV-2 inocculated Rhesus monkeys	Lung: caudal left lobe contains a 1 cm grey-red zone on the anterior medial aspect. Lymph nodes: Enlarged 3x normal
MA24	M	5.64	Mild cough (3), Slight increased effort breathing (20) Decreased appetite (3, 5, 7-9, 15, 16) Soft stool (4, 5, 8, 9, 16, 17, 20) Necropsy 21 dpi	 Neutrophila (4, 21), Eosinophilia (4, 21), Basophila (4, 14, 21) Lymphocytopenia (1), Monocytopenia (14) Neu/Lym ratio: 4.09 (1), 3.15 (4)	8-fold ↑ in CRP (1)	No significant gross abnormalities	Mild multifocal interstitial pneumonia with rare areas of pneumocyte hyperplasia and septal thickening. Findings could be compatible with a resolving viral pneumonia. Moderate to severe lymphoid hyperplasia was observed in the bronchial lymph node and tonsils. Proximal large intestine showed chronic inflammation compatible with chronic bacterial colitis	Lung: No gross lung lesions.
MA28	M	5.81	Slight increased effort breathing (8-12, 16, 19) Decreased appetite (7-9, 15, 16) Necropsy 21 dpi	 Neutrophilia (21), basophilia (21) Lymphocytopenia (4, 6), Monocytopenia (4, 14), Eosinopenia (4, 6)		Two small areas of consolidation in the left caudal lung lobe. Moderate mesenteric and mandibular lymph node enlargement	Mild interstitial pulmonary inflammation with minimal pneumocyte hyperplasia and rare fibrosis. Granulomatous inflammation within the left caudal lung, along with foreign debris, indicates subclinical aspiration pneumonia. The interstitial pneumonia is compatible with SARS-CoV-2 infection, but the character and severity suggest a resolving infection. Lymphoid tissues exhibited variable lymphoid hyperplasia. No evidence of thrombosis or vasculopathy was noted. Upper respiratory system also exhibited chronic inflammation that was a bit more active than the inflammation observed in the caudal respiratory tract.	Lung: Left caudal lung lobe contains 2-round, flat, pale tan foci ~1 cm in diameter on the dorsolateral surface at the level of the termination of the bronchial tree. Lymph nodes: Mesenteric and Mandibular 2x normal

Supplemental Table 1. Clinical, blood and necropsy observations in pigtail macaques (PTM) challenged with SARS-CoV-2 (n=4). Values in parenthesis represent days post SARS-CoV-2 Infection. Neutrophilia, eosinophilia, basophilia, monocytosis defined as ≥ 2-fold increase over baseline[16]. Lymphocytopenia, monocytopenia, eosinopenia, basopenia defined as a 35% reduction from baseline[16]. CRP: C-reactive protein

A. MA27

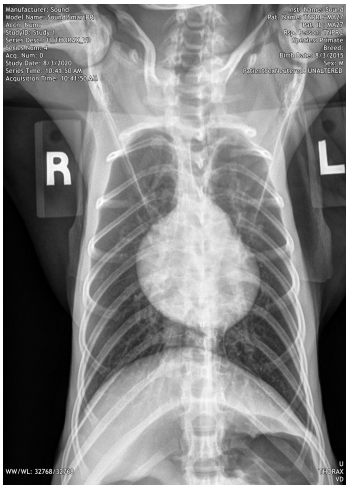

B.

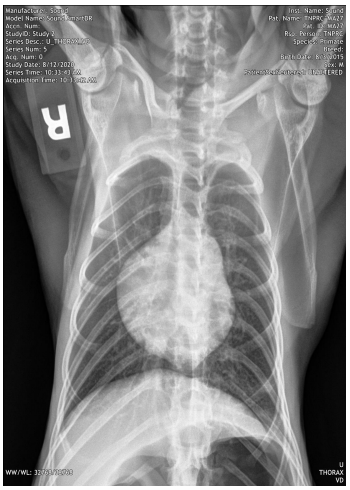

C. MA30

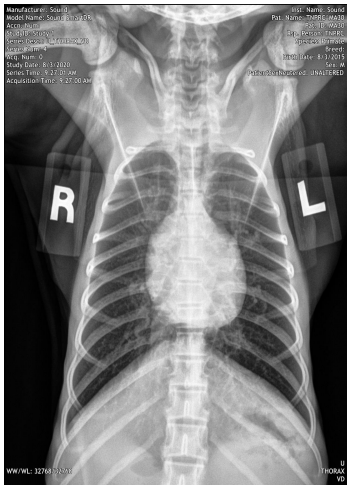

D.

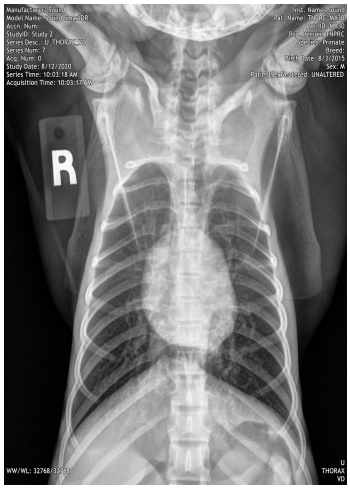

E. MA24

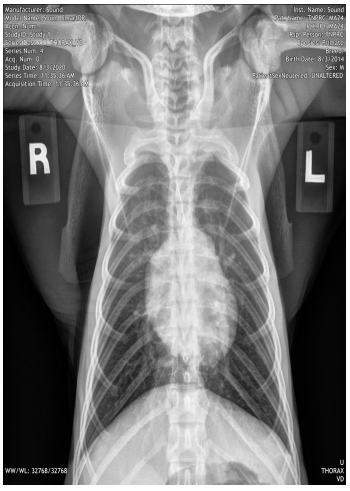

F.

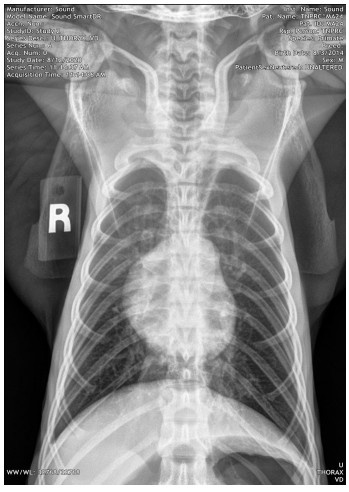

G.

H.

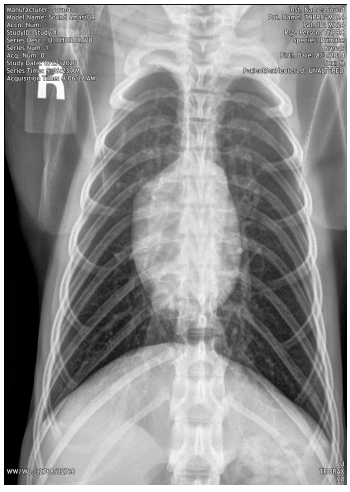

I. MA28

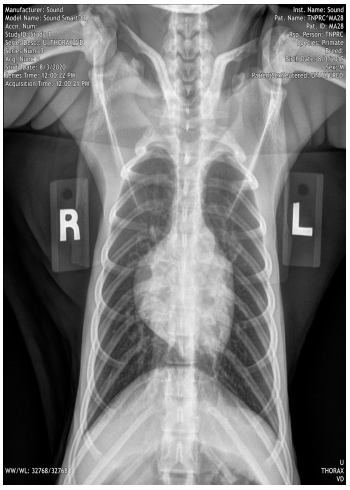

J.

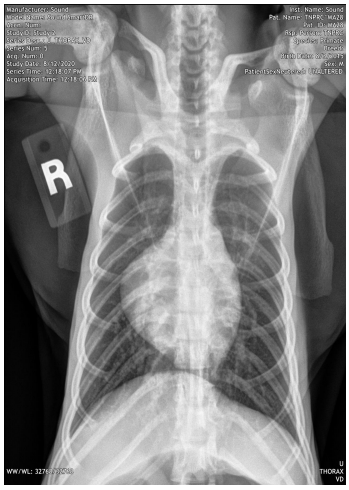

K.

L.

Supplemental Figure 1. **Radiographs of pigtail macaques (PTM) challenged with SARS-CoV-2.** MA27 baseline (**A**) and 6-days post infection (dpi) (**B**). MA30 at baseline (**C**) and 6-dpi (**D**). MA24 at baseline (**E**), 6-dpi (**F**), 14-dpi (**G**) and 21-dpi (**H**). MA28 at baseline (**I**), 6-dpi (**J**), 14-dpi (**K**) and 21-dpi (**L**). Baseline for all four PTM was established 3-days prior to infection.

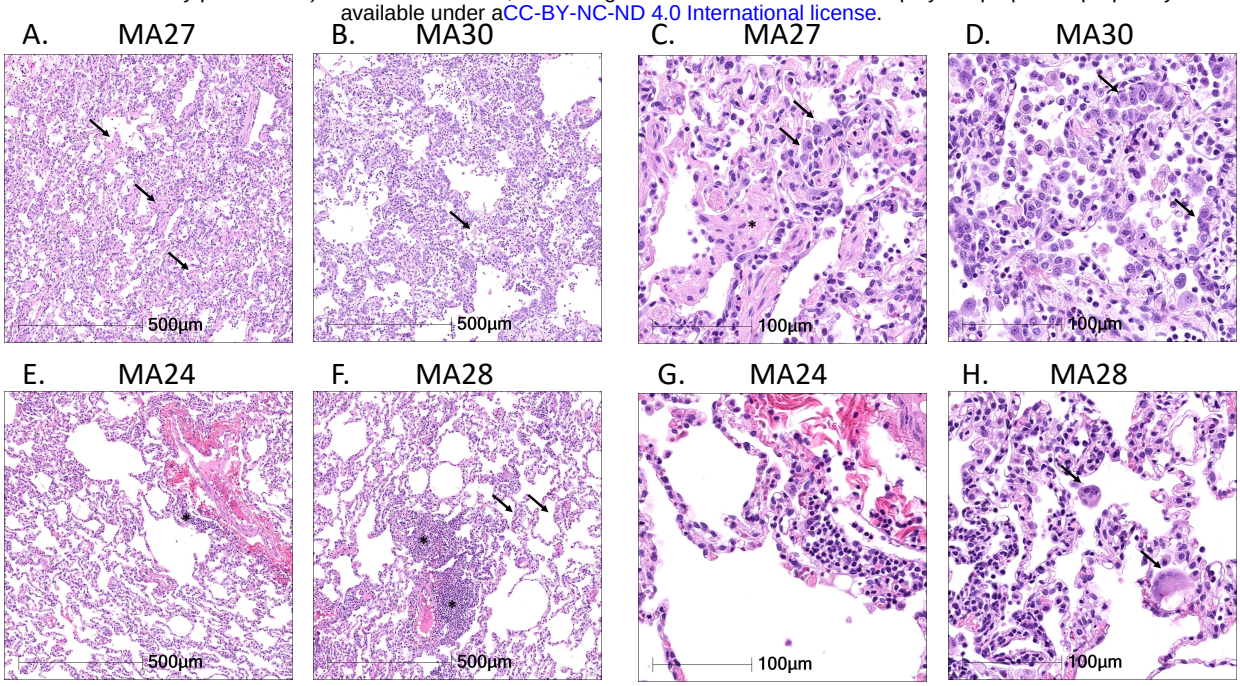

Figure 2. Histopathologic findings in SARS-CoV-2 infected pigtail macaques (PTM). Histopathologic findings at 6- **(A-D)** and 21-dpi **(E-H)**. **A&B.** At 6-dpi alveolar septa are expanded by inflammatory infiltrate and alveoli contain rafts of fibrin (**arrows**). **C&D.** The inflammatory infiltrate is composed of a mixture of histiocytes, lymphocytes, and neutrophils, and alveolar septa are frequently lined by type II pneumocytes (**arrows**). In severely affected areas, alveoli contain fibrin rafts (**C, asterisks**). **E&F.** At 21-dpi, there is residual inflammation composed of perivascular lymphoid aggregates (**asterisks**), and mild thickening of alveolar septa (**arrows). G&H**. The residual inflammation is composed predominately of lymphocytes, and in MA28, rare multinucleated giant cells (**H, arrows**).

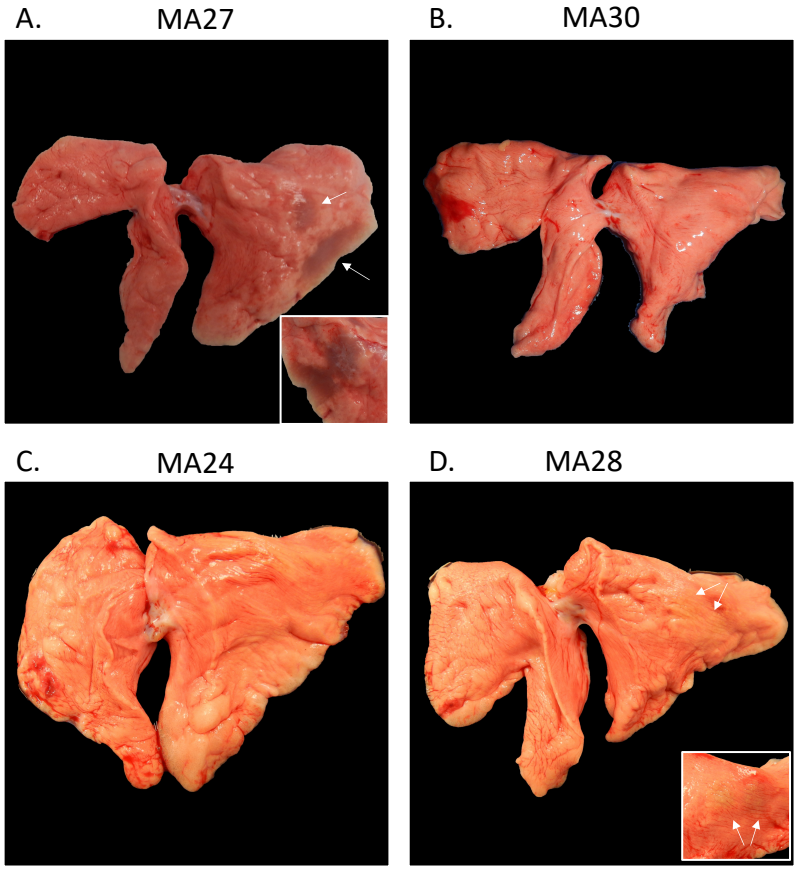

Supplemental Figure 2. Gross pathological pulmonary pathology in SARS-CoV-2 infected pigtail macaques (PTM). A-D. Gross pulmonary pathology at 6- (**A&B**) and 21-days post infection (dpi, **C&D**). **A**. MA27, the left caudal lung lobe has multifocal tan-plum areas of consolidation (arrows). Inset: the consolidation extends to the diaphragmatic and medial surface of the left caudal lung. There is no evidence of gross pathology in MA30 (B) or MA24 (C). **D.** MA28, the laterodorsal aspect of the left caudal lobe contains two small, flat tan foci (arrows). Inset: closer view of tan foci.

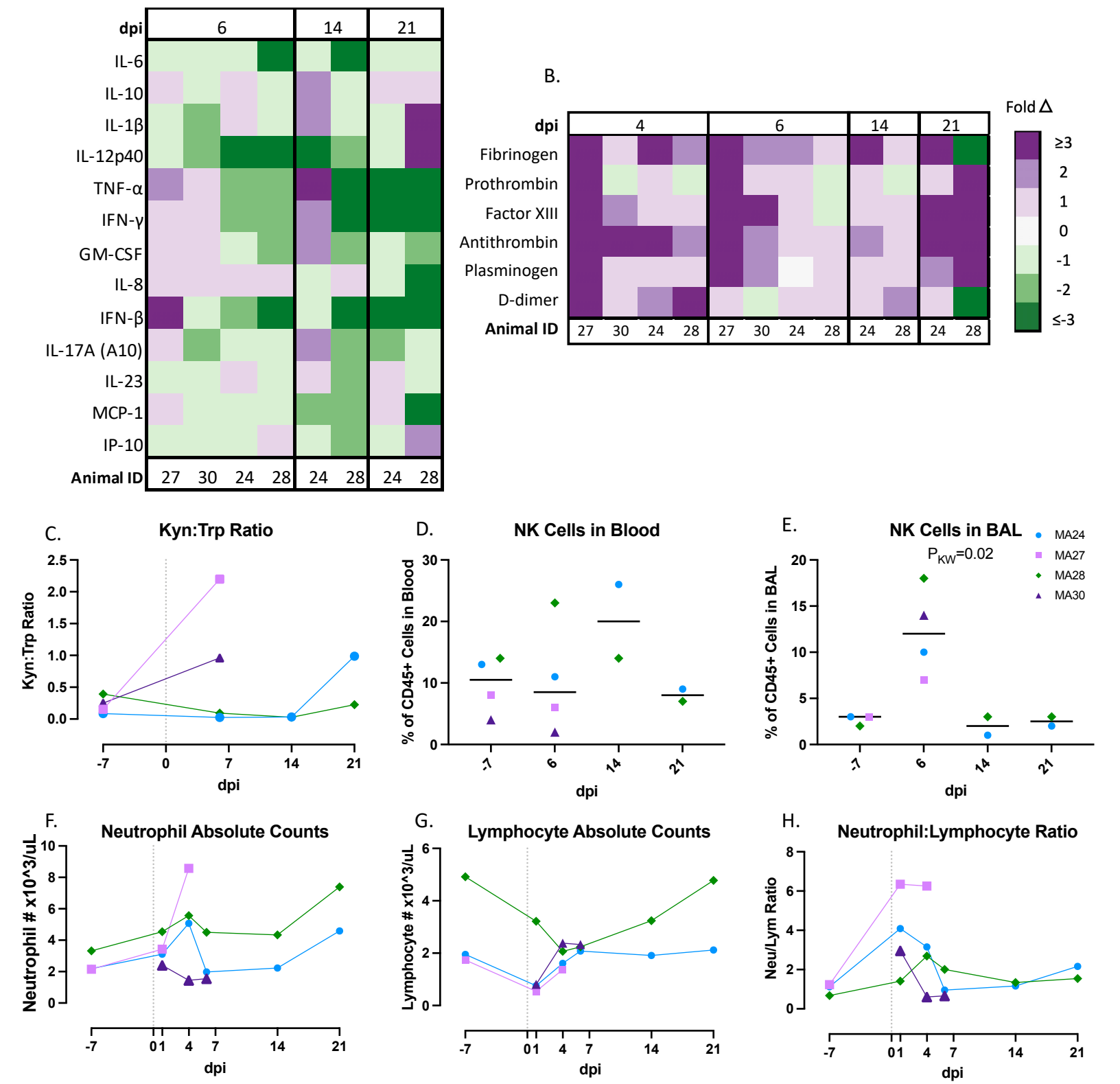

Figure 3. Inflammatory innate immune response in pigtail macaques challenged with SARS-CoV-2. A. Changes in serum cytokine levels at 6-, 14- and 21-days post SARS-CoV-2 infection. Data represent fold changes from baseline. **B.** Changes in coagulation biomarkers in plasma at 4-, 6-, 14- and 21-days post infection (dpi). Data are fold changes from baseline. **C.** Ratio of Kynurenine (Kyn) to Tryptophan (Trp) as a measure of indoleamine 2,3-dioxygenase (IDO) activity before and after SARS-CoV-2 infection. **D&E.** Frequency of Natural Killer (NK, CD45+ CD3- CD8+) cells in the blood (**D**) or **(E)** BAL at baseline, 6-, 14- and 21-days post infection (dpi). Bars represent median **F.** Absolute number of neutrophils pre- and post-SARS-CoV-2 infection. **G.** Absolute number of lymphocytes pre- and post-SARS-CoV-2 infection. **H.** Changes in neutrophil to lymphocyte ratio before and after SARS-CoV-2 infection. Figures 3C&D Baseline: n=4, Day 6: n=4, Day 14: n=2, Day 21: n=2; Figure 3E Baseline: n=3, Day 6: n=4, Day 14: n=2, Day 21: n=2; Figures 3F-H Baseline: n=3, Day 1: n=4, Day 4: n=4 Day 6: n=4, Day 14: n=2, Day 21: n=2. Figures C-H Day 0=day of infection. Kruskal-Wallis test for variance for overall medians used to determine significance. Kruskal-Wallis comparison of overall means (P_{KW}) test used to determine significance. P values ≤0.05 reported.

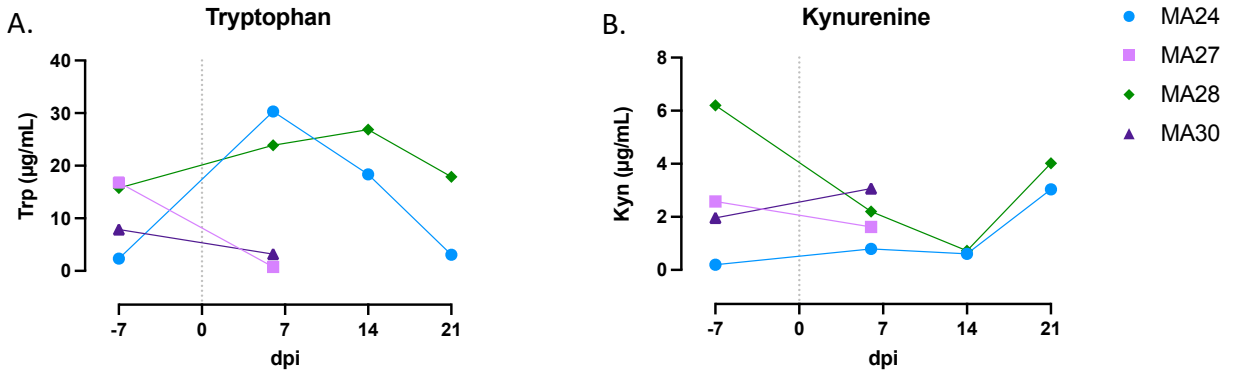

Supplemental Figure 3. Changes in IDO activity post SARS-CoV-2 Infection. A. Tryptophan (Trp) and **B.** Kynurenine (Kyn) levels in plasma before and after SARS-CoV-2 infection. Day 0=day of infection, Baseline: n=4, Day 7: n=4, Day 14: n=2, Day 21: n=2. dpi=days post infection.

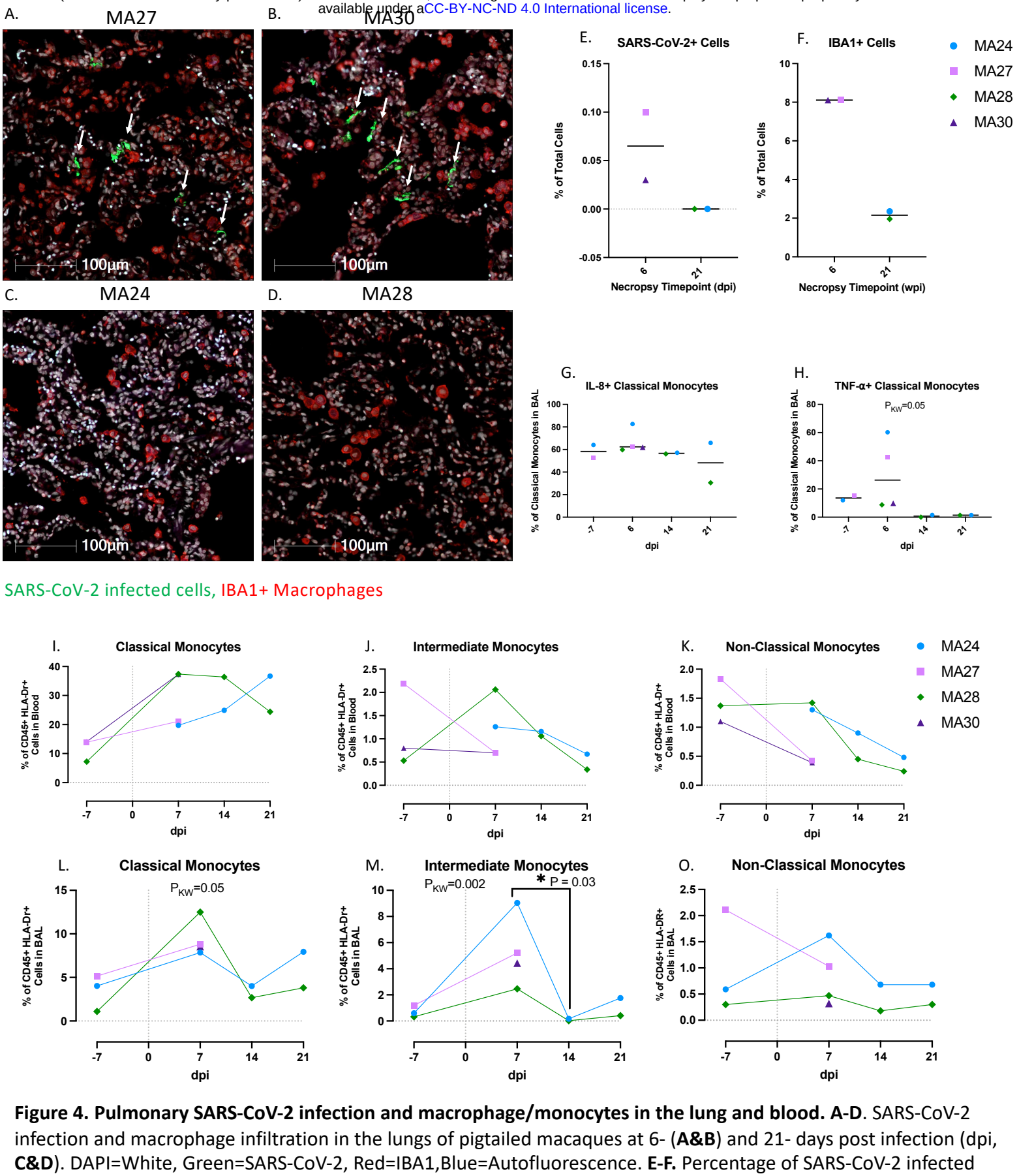

Figure 4. Pulmonary SARS-CoV-2 infection and macrophage/monocytes in the lung and blood. A-D. SARS-CoV-2 infection and macrophage infiltration in the lungs of pigtailed macaques at 6- (**A&B**) and 21- days post infection (dpi, **C&D**). DAPI=White, Green=SARS-CoV-2, Red=IBA1,Blue=Autofluorescence. **E-F.** Percentage of SARS-CoV-2 infected cells (**E**) and IBA1+ macrophages (**F**) in the lung at necropsy. Bars represent median. **G&H**. Frequency of IL-8 (**G**) and TNF-α (**H**) expressing classical monocytes (CD45+ HLA-DR+ CD14- CD16+) in BAL. **I-O.** Classical (**I&L**) intermediate (CD45+ HLA-DR+ CD14+ CD16+) (**J&M**), and non-classical monocytes (CD45+ HLA-DR+ CD14- CD16+) (**K&O**) frequencies in the blood and BAL before and after SARS-CoV-2 infection. Day 0=day of infection. I-O Baseline (day -7): n=3, Day 6: n=4, Day 14: n=2, Day 21: n=2. Kruskal-Wallis comparison of overall means (P_{KW}) and Dunn's Multiple comparisons (designated by line, P_D) tests used to determine significance. P values ≤0.05 reported

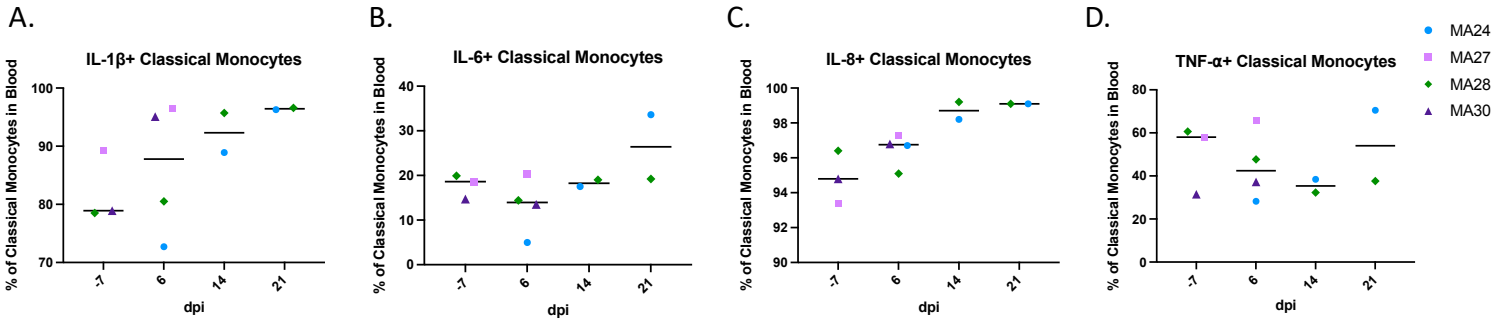

Figure 5. A-D. Monocyte cytokine response in the blood of pigtail macaques challenged with SARS-CoV-2. Frequency of IL-1β (**A**), IL-6 (**B**), IL-8 (**C**) and TNF-α (**D**) expressing classical monocytes (CD45+ HLA-DR+ CD14- CD16+) in the blood. Bars represent median. Day 0=day of infection. Baseline (-7): n=3, Day 6: n=4, Day 14: n=2, Day 21: n=2.

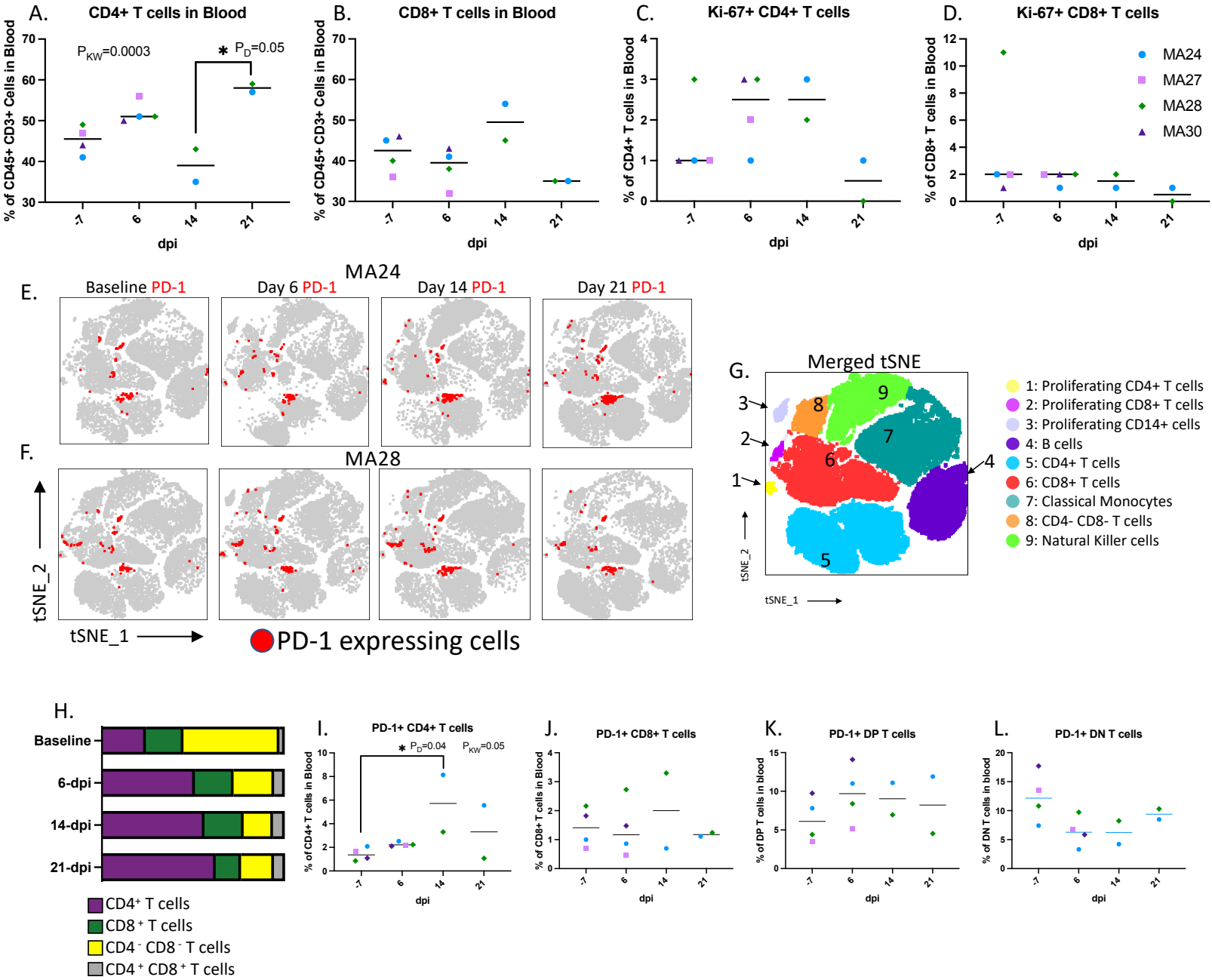

Figure 6. T cells in the blood. **A-B.** CD4+ (**A**) and CD8+ (**B**) T cell frequencies in the blood before and 1-, 2-, and 3-weeks post SARS-CoV-2 infection. **C-D.** Changes in Ki-67 expressing CD4+ (**C**) and CD8+ (**D**) T cells. Bars represent median **E.** tSNE plots displaying changes in PD-1 expression (red) in peripheral CD45+ cells overtime. MA24 (**E**) and MA28 (**F**) displayed as a representative animals. **G.** Merged tSNE indicating phenotype of the tSNE defined cell populations in E. **H.** Average changes in the percentages of CD4+, CD8+, CD4- CD8- (DN) and CD4+ CD8+ (DP) T cells within the total PD-1+ CD3+ cell population. **I-L.** Frequency of PD-1+ expressing CD4+ (**I**), CD8+ (**J**), DP (**K**) and DN (**L**) T cells in the blood. Bars represent median. Kruskal-Wallis comparison of overall means (P_{KW}) and Dunn's Multiple comparisons (designated by line, P_D) tests used to determine significance. P values ≤0.05 reported. Baseline (-7): n=4, Day 6: n=4, Day 14: n=2, Day 21: n=2.

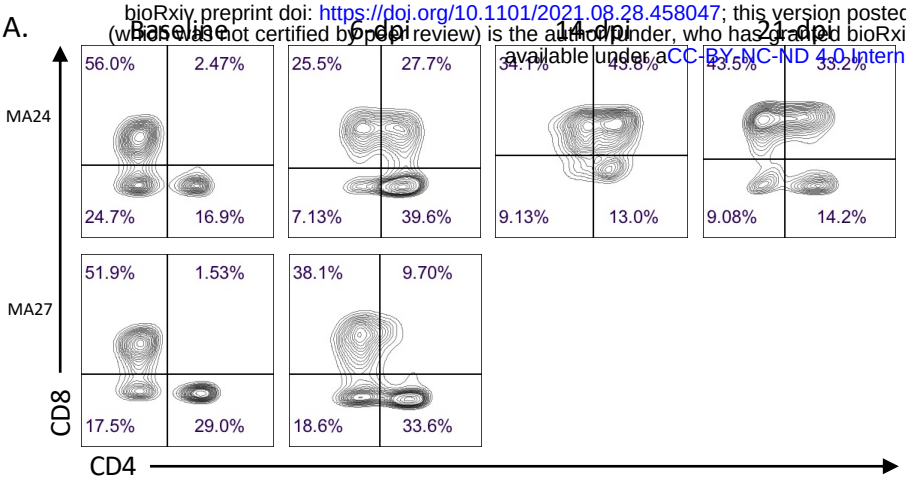

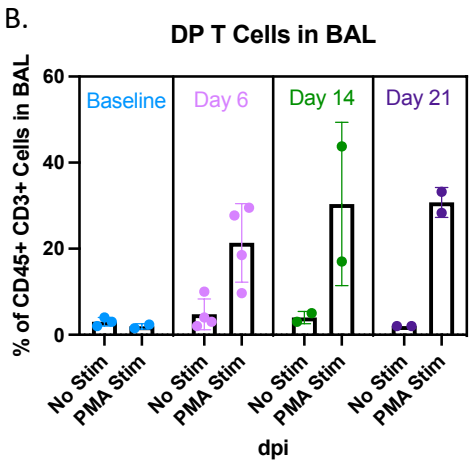

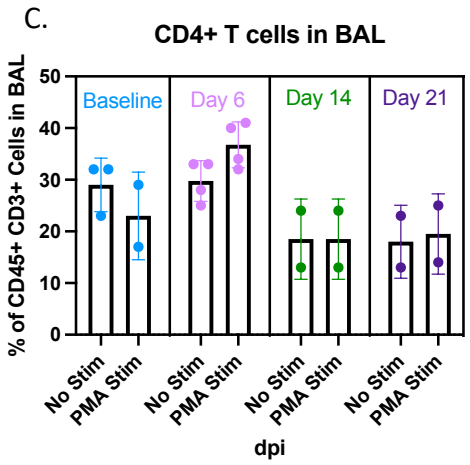

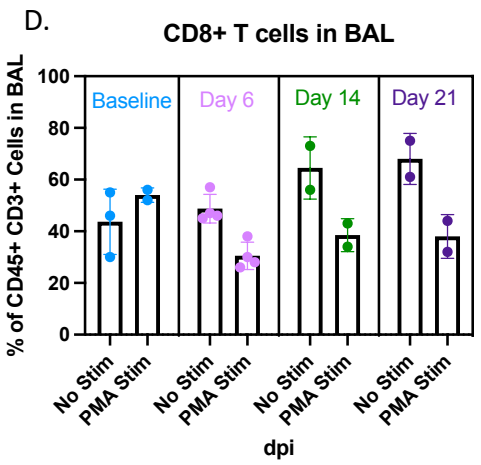

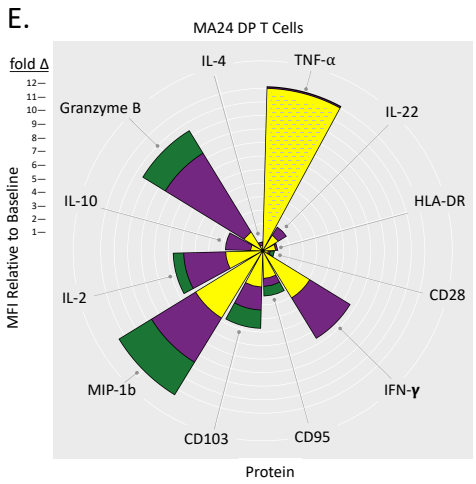

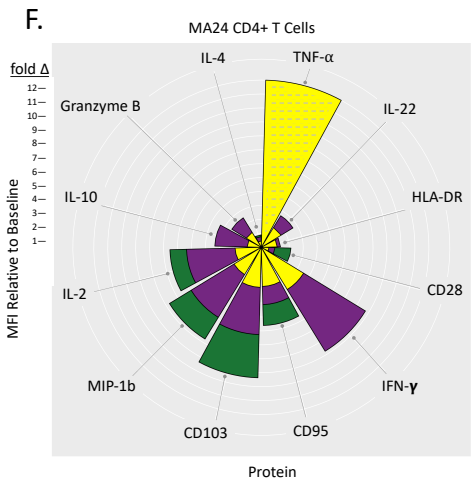

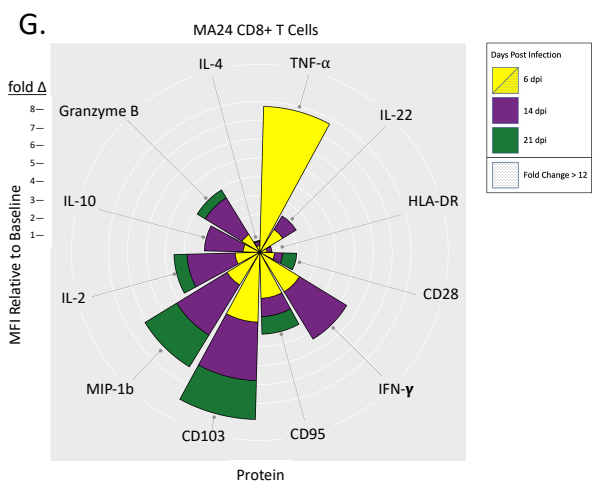

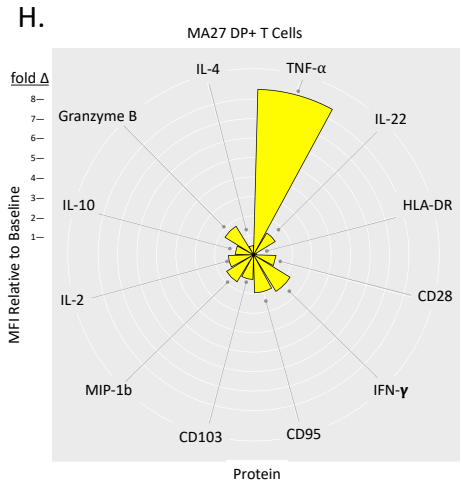

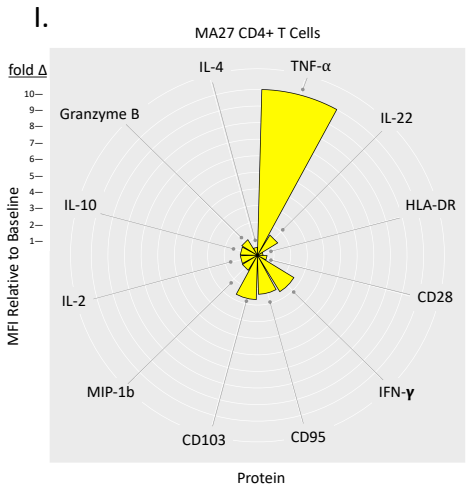

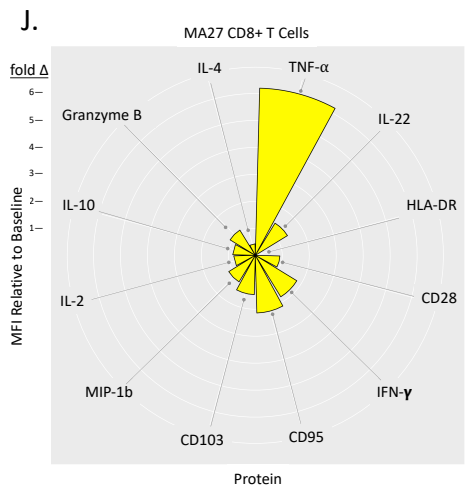

Figure 7. Adaptive T cell responses in the BAL. **A.** Representative flow cytometry plots showing changes in CD4 and CD8 expression in PMA/ionomycin stimulated CD3+ cells in BAL. Two animals shown (MA24 necropsied at 21-dpi, MA27 necropsied at 6-dpi). **B-D.** Effect of PMA/ionomycin on the frequency of CD4+ CD8+ (DP, **B**) CD4+ (**C**) and CD8+ (**D**) T cells in BAL before and 6-, 14-, and 21-days post SARS-CoV-2 infection. Bars represent mean and standard deviation. **E-J.** Nightingale Rose Plots (NRPs) showing fold changes in cytokine and surface protein expression compared to baseline (MFI). Yellow=6-dpi, Purple=14-dpi, Green=21-dpi. Size of petals represents magnitude of increase in expression. Distance from one white ring to the next is a 1-fold change. A decrease in expression is represented by a petal size less than the distance between two rings. Two animals shown (MA24 necropsied at 21-dpi, MA27 necropsied at 6-dpi). At 6-dpi, MA24 DP T cell TNF-α MFI is 24x baseline and CD4+ T cell TNF-α MFI is 50x baseline. Graph cutoff is set to a 12-fold change. **B-D.** Baseline: n=3 (No Stimulation (Stim)) and n=2 (Stim), Day 6: n=4 (No Stim) and n=4 (Stim), Day 14: n=2 (No Stim) and n=2 (Stim), Day 21: n=2 (No Stim) and n=2 (Stim).

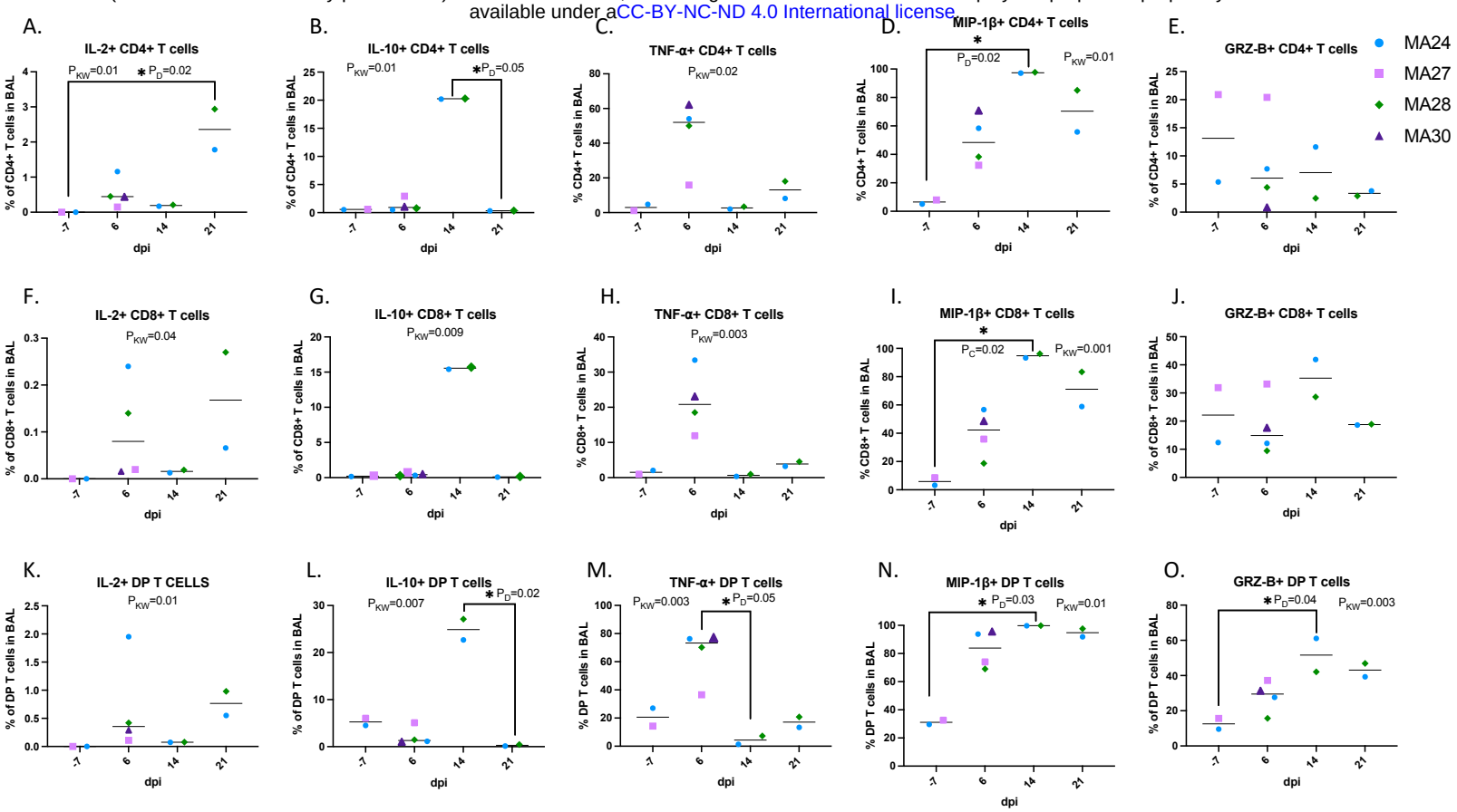

Figure 8. Changes in T cell cytokine expression in the lung. A-O. PMA/ionomycin stimulated CD4+ T cells (**A-E**), CD8+ T cells (**F-J**), and CD4+ CD8+ (DP) T cells (**K-O**). Bars represent median. Kruskal-Wallis comparison of overall means (P_{KW}) and Dunn's Multiple comparisons (designated by line, P_D) tests used to determine significance. P values ≤0.05 reported. Baseline (-7): n=2, Day 6: n=4, Day 14: n=2, Day 21: n=2.

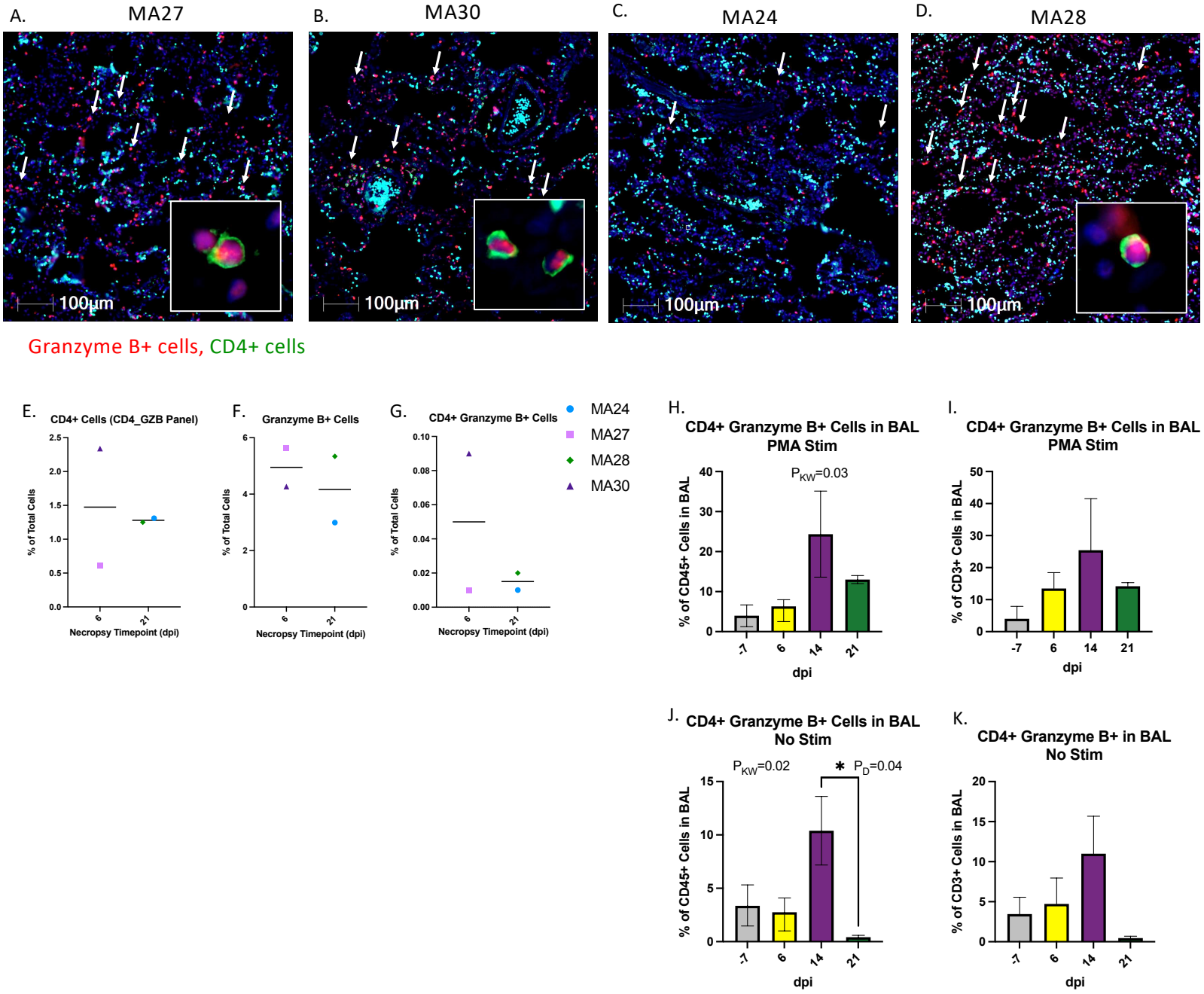

Figure 9. CD4 and Granzyme B expression in the lungs of SARS-CoV-2 infected macaques at 6- (A&B) and 21-days post infection (dpi, C&D). At 6-dpi, MA27 (**A**) and MA30 (**B**) the lungs are infiltrated by large numbers of Granzyme B positive cells (red, arrows). Insets: Rare CD4+ cells (green) exhibit granzyme expression. At 21-dpi, MA24 (**C**) exhibits low numbers of Granzyme B positive cells (red, arrows) compared to MA28 (**D**) and the two, 6-dpi animals (**A&B**). DAPI=Blue, Green=CD4, Red=Granzyme B. **E-G.** Percentage of CD4+ (**E**), Granzyme B+ (**F**) and CD4+ Granzyme B+ (**G**) cells in the lung at necropsy. Bars represent median. **H-K.** CD4+ Granzyme B+ T cells (CD45+ CD3+ CD4+ Granzyme B+) in BAL at Baseline (-7) and 6-, 14- and 21-dpi as a percentage of CD45+ cells (**H&J**) and CD3+ cells (**I&K**). **H&I**. Mononuclear cells, isolated from BAL, were stimulated with PMA/ionomycin for 4-6 hours. Bars represent median and standard deviation. Kruskal-Wallis comparison of overall means (P_{KW}) and Dunn's Multiple comparisons (designated by line, P_D) tests used to determine significance. P values ≤0.05 reported. **H-K**. Baseline: n=3 (No Stimulation (Stim)) and n=2 (Stim), Day 6: n=4 (No Stim) and n=4 (Stim), Day 14: n=2 (No Stim) and n=2 (Stim), Day 21: n=2 (No Stim) and n=2 (Stim).

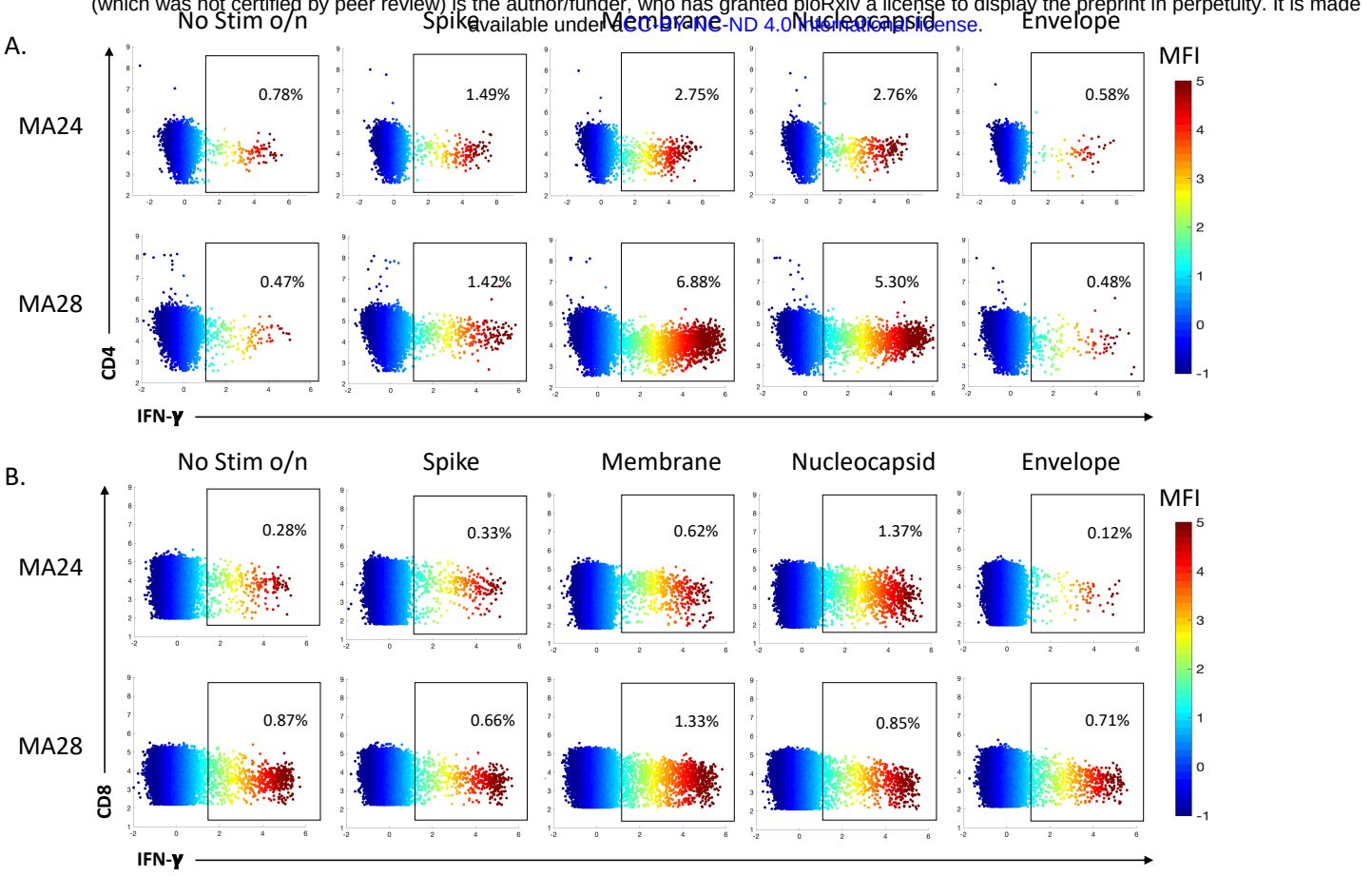

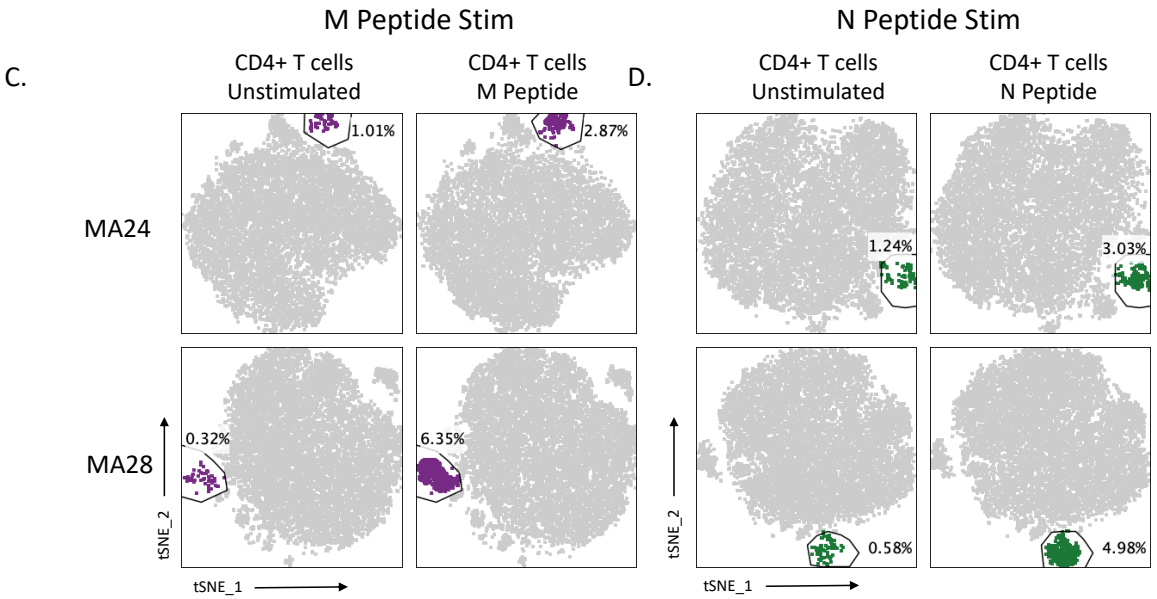

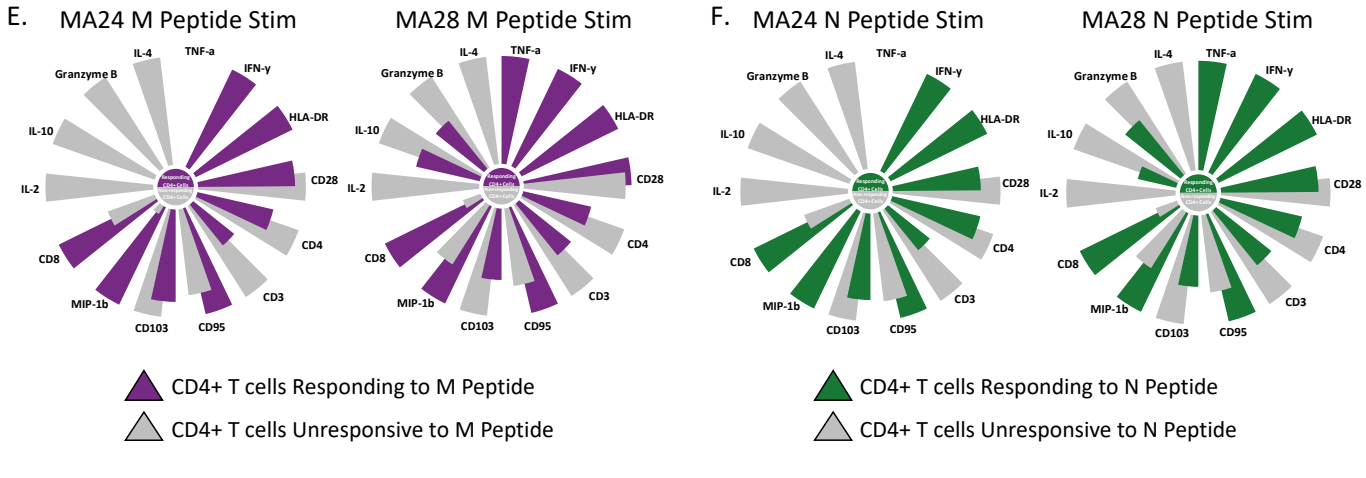

Figure 10. SARS-CoV-2 peptide specific T cell response in the lung 21-days post infection. Two animals shown (MA24 & MA28 necropsied 21-dpi) **A&B.** Flow cytometry dot plots showing CD4+ (**A**) and CD8+ (**B**) T cell Interferon-γ (IFN-γ) response to overnight SARS-CoV-2 peptide (spike, membrane, nucleocapsid and envelope) stimulation. No stim o/n=cells incubated overnight without stimulation. Heatmap represents arcsin transformed MFI values. **C&D.** tSNE plots of CD4+ T cells showing an expansion in cells following overnight peptide stimulation. M=SARS-CoV-2 membrane peptides (**C**), N=SARS-CoV-2 nucleocapsid peptides (**D**). **E&F.** Radial bar plot comparing MFI values of the expanded CD4+ T cell population gated on in **C&D** to the unchanged CD4+ population within the same tSNE plot. Representative animals MA24, MA28 (necropsied at 21-dpi). The higher MFI value is set to 100 and the percent difference is calculated between the higher and lower MFI values. Size of the petals represent this analysis.

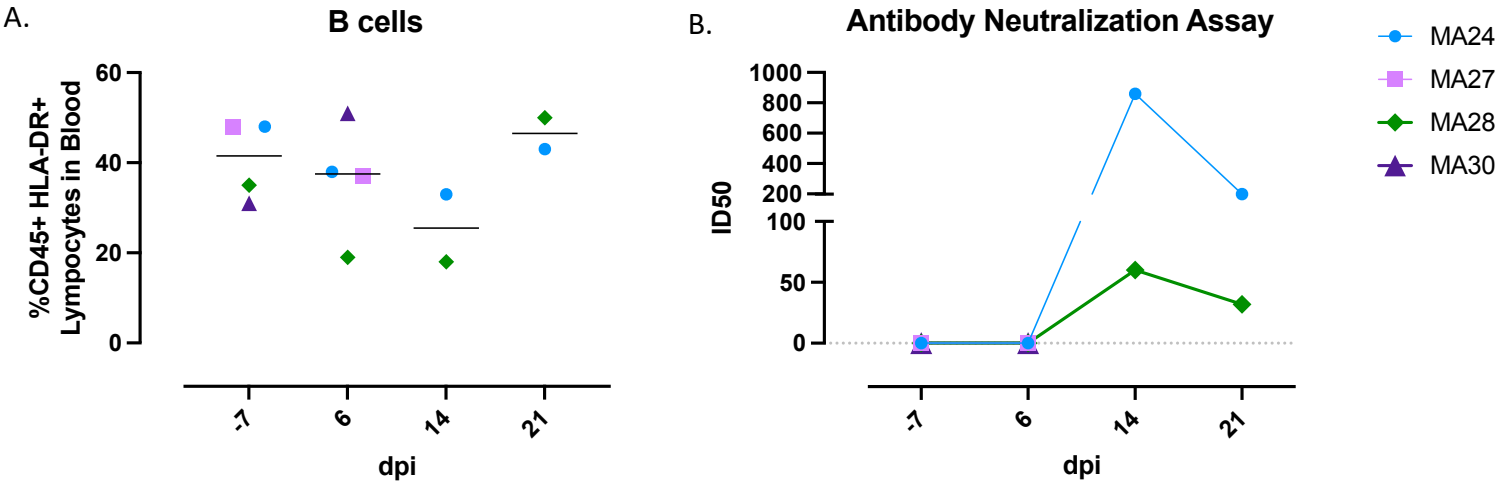

Figure 11. Humoral immune response in SARS-CoV-2 infected pigtail macaques. A. B cell frequencies in the blood before and 6-, 14-, and 21-days post (dpi) SARS-CoV-2 infection. Bars indicate median. **B.** Pseudovirus neutralization assay showing serum antibody levels against SARS-CoV-2 using HEK 293T/ACE2 cells. Baseline (-7): n=4, Day 6: n=4, Day 14: n=2, Day 21: n=2

Supplemental Table 2. Monocyte Panel

Fluorochrome	Antigen	Volume (uL)/Test	Clone	Catalog#	Lot#	Company
FITC	IL-6*	5	MQ2-6A3	554696	6168973	BD Pharmingen
PCP-Cy5.5	CD169	5	7-239	346020	B309159	BioLegend
AL647	IL-1B*	5	JK1B-1	508208	B274564	BioLegend
AL700	TNF-a*	5	MAb11	502928	B221571	BioLegend
APC-Cy7	HLA-DR	5	L243	307618	B295253	BioLegend
PacBlue	CD66	2	TET2	130-119-851	1320070484	Miltenyi Biotec
BV510	L/D	0.5	Fixable Aqua Dead Cell Stain Kit	L34957		Invitrogen
BV605	CD45	5	D058-1283	564098	9051992	BD Horizon
BV650	CD11c	5	S-HCL-3	744437	0203626	BD OptiBuild
BV711	CD16	5	3G8	302044	B296475	BioLegend
BV786	CD103	5	Ber-ACT8	350230	B274642	BioLegend
PE-CF594	IL-8*	5	G265-8	563531	0219387	BD Horizon
PE-Cy7	CD68*	5	Y1/82A	565595	0079803	BD Pharmingen
BUV395	CD123	5	7G3	564195	9337379	BD Horizon
BUV496	CD206	5	19.2	741173	0261803	BD OptiBuild
BUV737	CD14	5	M5E2	612764	0140605	BD Horizon

Supplemental Table 3. Phenotype Panel

Fluorochrome	Antigen	Volume (uL)/Test	Clone	Catalog#	Lot#	Company
FITC	CD21	5	B-Ly4	561372	0149866	BD Pharmingen
PCP-Cy5.5	CD169	5	7-239	346020	B309159	BioLegend
APC	CD11c	5	S-HCL-3	340714	70397	BD Pharmingen
AL700	Ki67*	5	B56	561277	9261927	BD Pharmingen
APC-Cy7	CD20	5	L27	561277	8320624	BD Bioscience
PacBlue	CD8	5	SK1	344718	B280004	BioLegend
BV510	L/D	0.5	Fixable Aqua Dead Cell Stain Kit	L34957		Invitrogen
BV605	CD4	5	OKT4	317438	B297647	BioLegend
BV650	CD3	5	SP34-2	563916	D163859	BD Horizon
BV711	CD16	5	3G8	302044	B296475	BioLegend
BV785	CD27	5	O323	302832	B264783	BioLegend
PE	FasL	5	NOK-1	306407	B269886	BioLegend
PE-CF594	HLA-DR	5	L243	307654	B320176	BioLegend
PE-Cy5	CD95	5	DX2	15-0959-42	2252537	Invitrogen
PE-Cy7	PD-1 (CD279)	5	J105	25-2799-42	228650	Invitrogen
BUV395	CD45	5	D058-1283	564099	0192257	BD Horizon
BUV496	CD28	5	CD28.2	741168	0203628	BD OptiBuild
BUV737	CD14	5	M5E2	612764	0140605	BD Horizon

* Intracellular

Supplemental Table 4. T cell Panel

Fluorochrome	Antigen	Volume (uL)/Test	Clone	Catalog#	Lot#	Company
FITC	MIP-1b*	20	D21-1351	560565	348912	BD Parmingen
PCP-Cy5.5	IL-2*	5	MQ1-17H12	560708	8142599	BD Parmingen
AL647	IFN-g*	5	4S-B3	502516	B228928	BioLegend
AL700	TNF-a*	5	MAb11	557996	8179967	BD Parmingen
APC-Cy7	HLA-DR	5	L243	307618	B295253	BioLegend
PacBlue	CD8	5	SK1	344718	B280004	BioLegend
BV510	Live/Dead	0.5	Fixable Aqua Dead Cell Stain Kit	L34957		Invitrogen
BV605	CD4	5	OKT4	317438	B297647	BioLegend
BV650	CD3	5	SP34-2	563916	D163859	BD Horizon
BV711	CD95	5	DX2	563132	004458	BD Horizon
PE	IL10*	5	JES3-9D7	501404	B273796	BioLegend
PE-CF594	GZB*	5	GB11	562462	0050626	BD Horizon
PE-Cy7	IL-4*	5	MP4-25D2	500824	B293168	BioLegend
BUV395	CD45	5	D058-1283	564099	0101778	BD Horizon
BUV496	CD28	5	CD28.2	741168	0203628	BD OptiBuild

* Intracellular

Supplemental Table 5. T cell SARS-CoV-2 Peptide, PMA/Ionomycin Stimulation

Stimulant	Volume (uL)/mL	Catalog#	Lot#	Company
Cell Stimulation Cocktail	1	423301	B295704	BioLegend
SARS-CoV-2 Spike Peptide	10	NR-52402		BEI Resources, NIAID, NIH
SARS-CoV-2 Membrane Peptide	5	NR-53822		BEI Resources, NIAID, NIH
SARS-CoV-2 Nucleocapsid Peptide	5	NR-52419		BEI Resources, NIAID, NIH
SARS-CoV-2 Envelope Peptide	5	NR-53822		BEI Resources, NIAID, NIH
Brefeldin-A	1	420601	B211242	BioLegend

Supplemental Table 6. Immunohistochemistry

Primary Antibody	Species	Company	Catalog#	Dilution	Secondary Antibody	
					Species	Fluorochrome
SARS	Guinea Pig	BEI	NR-10361	1:1000	Goat anti-guinea pig	Alexa Fluor488
IBA1	Rabbit	Wako	019-19741	1:50	Goat anti-Rabbit	Alexa Fluor568
CD3	Mouse IgG1	Agilent	M7254	1:20	Goat anti-MS IgG1	Alexa Fluor568
CD4	Rabbit	Abcam	Ab133616	1:10	Goat anti-Rabbit	Alexa Fluor488
Granzyme	Mouse IgG2a	Agilent	M7235	1:50	Permanent Red (Agilent K0640)	
Dapi		Invitrogen	D1306	1:20,000		

639 Queen St. W Suite 401
Toronto ON M5V 2B7 Canada
www.biorender.com

Confirmation of Publication and Licensing Rights

August 25th, 2021
Science Suite Inc.

Subscription:	*Student Plan Promo (Legacy)*
Agreement number:	*IA22VLXDAV*
Journal name:	*PLOS Pathogens*

To whom this may concern,

This document is to confirm that **Alex Melton** has been granted a license to use the BioRender content, including icons, templates and other original artwork, appearing in the attached completed graphic pursuant to BioRender's Academic License Terms. This license permits BioRender content to be sublicensed for use in journal publications.

All rights and ownership of BioRender content are reserved by BioRender. All completed graphics must be accompanied by the following citation: "Created with BioRender.com".

BioRender content included in the completed graphic is not licensed for any commercial uses beyond publication in a journal. For any commercial use of this figure, users may, if allowed, recreate it in BioRender under an Industry BioRender Plan.

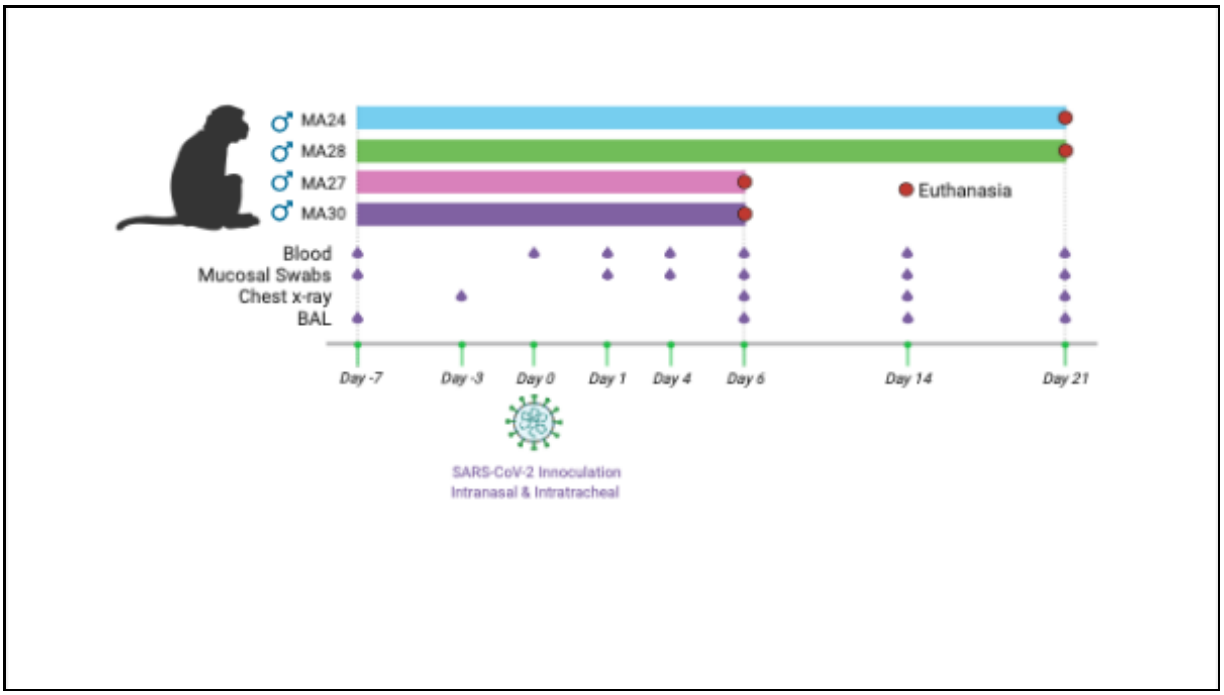

For any questions regarding this document, or other questions about publishing with BioRender refer to our BioRender Publication Guide, or contact BioRender Support at support@biorender.com.